Targeting of ibrutinib resistance–driving pathways by miR-28 in ABC-DLBCL

Emigdio Álvarez-Corrales[1], Carmen Gómez-Escolar[2,3*], Rocío Moreno-Palomares[1*], Mario Martínez[4*], María Laguna-Herrero[1], Teresa Fuertes[1,2,5], Belén S. Estrada[6], Sonia Mur[2], Nuria Martínez-Martín[6], Álvaro Somoza[4], Almudena R. Ramiro[2] and Virginia G. de Yébenes[1]

[1] Dept. of Immunology, Ophthalmology and ENT, Universidad Complutense de Madrid; Instituto de Investigación Sanitaria Hospital 12 de Octubre (imas12), Madrid, Spain
[2] B Cell Biology Lab. Centro Nacional de Investigaciones Cardiovasculares (CNIC), Madrid, Spain
[3] Current adress: Instituto de Neuorociencias de Alicante (CSIC), Alicante, Spain
[4] Instituto Madrileño de Estudios Avanzados en Nanociencia (IMDEA Nanociencia), Madrid, Spain

[5] Current adress: Department of Pharmacy and Nutrition. Faculty of Biomedical and Health Sciences.Universidad Europea de Madrid, Spain.

[6] Centro de Biología Molecular Severo Ochoa (CSIC), Madrid, Spain

* These authors contributed equally to the work

Corresponding author: Virginia G de Yébenes Universidad Complutense de Madrid. Pza. Ramón y Cajal, s/n. 28040 Madrid. Phone# 34 91 394 1641. E-mail: vgarciay@ucm.es

Conflict of interest: The authors declare no potential conflicts of interest

ABSTRACT

Diffuse large B-cell lymphoma (DLBCL) is the most common aggressive B-cell lymphoma. Although many patients respond well to R-CHOP immunochemotherapy, those with the activated B-cell (ABC) subtype are often refractory or relapse. Bruton tyrosine kinase (BTK) inhibitors such as ibrutinib have improved outcomes, but acquired resistance limits their long-term efficacy. Here, we modeled the development of ibrutinib resistance in ABC-DLBCL and investigated whether the BCR-signaling regulator microRNA-28 (miR-28) can block this process. Using flow cytometry–based competition assays, multicolor clonal barcoding, transcriptomic profiling, and xenograft models, we found that miR-28 expression impairs the emergence of ibrutinib-resistant ABC-DLBCL cells. Mechanistically, miR-28 interferes with the clonal selection process triggered by ibrutinib treatment and rewires transcriptional programs by downregulating mitochondrial and mTOR signaling pathways critical for resistance development. Furthermore, lower expression of genes that we identified as repressed by miR-28 correlates with improved survival in ibrutinib-treated patients aged over 60 years from the PHOENIX trial cohort with the MCD genetic subtype, which is associated with ABC-DLBCL. Finally, we show that the targeted therapeutic delivery of miR-28 via aptamer-guided nanoparticles suppresses ibrutinib-resistant tumor growth *in vivo*. These findings identify miR-28 as an effective inhibitor of ibrutinib resistance, underscoring its translational potential as an adjunct strategy in ABC-DLBCL therapy.

INTRODUCTION

Diffuse large B-cell lymphoma (DLBCL) is the most common aggressive B-cell lymphoma, accounting for nearly 40% of all B-cell lymphomas[1]. DLBCL patients are generally treated with a chemotherapy-based regimen consisting of rituximab plus cyclophosphamide, doxorubicin, vincristine, and prednisone (R-CHOP). Recent studies have aimed to define the molecular heterogeneity of DLBCL to support the development of targeted therapies. Based on gene expression profiling, DLBCL is classified into two main subtypes: germinal center B cell-like (GCB) and activated B cell-like (ABC), the latter is characterized by the expression of genes induced upon B-cell receptor (BCR) activation and is associated with a worse prognosis than GCB-DLBCL[2]. Genetic profiling has identified distinct subtypes within ABC-DLBCL—primarily MCD, BN2, and N1—which differ not only in their genetic alterations but also in clinical outcomes[3]. Overall survival after R-CHOP chemotherapy is achieved in only 40% of ABC-DLBCL patients and in as few as 26% of those with the MCD genetic subtype[3, 4]. Functional genomic screens have identified genes essential for oncogenic signaling in DLBCL, including genes encoding proximal BCR signaling components as well as genes involved in distinct downstream survival pathways such as PI3K/AKT/mTOR and NF-κB. These screens have also revealed that ABC-DLBCL, but not GCB-DLBCL, is highly dependent on BCR-mediated NF-κB signaling for survival[5, 6, 7, 8].

The introduction of Bruton's tyrosine kinase (BTK) inhibitors, such as ibrutinib, which blocks BCR-dependent NF-κB activation, has been transformative in the treatment of several B-cell malignancies, including chronic lymphocytic leukemia (CLL)[9]. Clinical trials have also demonstrated the potency of BTK inhibition, either as monotherapy or in combination with R-CHOP, in ABC-DLBCL[10, 11, 12, 13, 14]. However, responses to ibrutinib

in ABC-DLBCL are variable or incomplete across different age groups and genetic subtypes, and acquired resistance remains a significant barrier to achieving durable outcomes[10, 14]. Prolonged ibrutinib treatment has been associated with the emergence of resistance, and mutations affecting BTK, its downstream effector PLCG2, or CARD11 have been identified in CLL and DLBCL patients[10, 15, 16, 17, 18]. Importantly, beyond these genetic alterations, resistance also emerges through non-genetic mechanisms, such as rewiring of oncogenic signaling pathways and feedback activation of compensatory survival programs[19, 20, 21]. Addressing these adaptive responses to ibrutinib treatment requires rational combinations of targeted therapies designed to inhibit different resistance-promoting pathways simultaneously.

In this context, microRNAs (miRNAs) have gained increasing attention as potential therapeutics for B-cell malignancies. miRNAs are small non-coding RNAs that regulate gene expression post-transcriptionally by binding imperfectly to target messenger RNAs (mRNAs), resulting in mRNA degradation or translational inhibition. Each miRNA can modulate the expression of multiple mRNAs, thereby influencing complex gene regulatory networks[22]. During oncogenesis, miRNA-mediated regulation is frequently disrupted. Several miRNAs have been identified as key contributors to B-cell lymphoma pathogenesis, functioning as either tumor suppressors or oncogenic miRNAs[23].

Recent advances have enabled the modulation of miRNA activity through the delivery of synthetic mimics or inhibitors, offering new therapeutic opportunities for various diseases, including cancer. In this context, miRNA-based therapies have emerged as promising alternatives to conventional treatments for B-cell non-Hodgkin lymphoma (B-NHL) and other malignancies[24, 25, 26]. A key advantage of these strategies is their ability to simultaneously target multiple components of oncogenic signaling pathways,

potentially limiting the emergence of resistance mechanisms such as mutations in individual oncogenes.

miR-28 is a microRNA whose expression is downregulated in B cell lymphomas[27]. We previously reported that it targets a BCR-dependent signaling network in B cells and exerts anti-tumor effects in DLBCL, both as a single agent and in combination with ibrutinib[28, 29]. In the present study, we evaluated the role of miR-28 in preventing the emergence of ibrutinib resistance. Our findings show that miR-28 disrupts the post-transcriptional adaptation and clonal selection processes that occur during the development of resistance to ibrutinib in ABC-DLBCL. Moreover, we describe the synthesis and *in vivo* antitumor efficacy of CD19/CD20-aptamer–functionalized gold nanoparticles (AuNPs) that efficiently deliver a miR-28 mimic to resistant DLBCL cells, achieving sustained tumor growth suppression.

MATERIALS AND METHODS

Cell lines and cell culture

Human ABC-DLBCL cell lines (MD-901, Riva, HBL1, and U2932) were cultured in RPMI medium supplemented with 10% fetal bovine serum, 1% penicillin/streptomycin, and 10 mM HEPES (Gibco), at 37 °C in the presence of 5% CO_2. All cell lines were routinely tested and confirmed to be mycoplasma-free using the MycoAlert™ PLUS Mycoplasma Detection Kit (Lonza).

Mice

Non-obese diabetic severe combined immunodeficiency G (NOD/SCID/IL-2rγnull; NSG) mice were housed at the Centro Nacional de Investigaciones Cardiovasculares (CNIC). All animal procedures were conducted in accordance with EU Directive 2010/63/EU and Recommendation 2007/526/EC on the protection of animals used for scientific purposes, as implemented in Spanish law under Royal Decree 53/2013. All protocols were reviewed by the CNIC Institutional Animal Care and Use Committee (IACUC) and approved by the *Consejería de Medio Ambiente, Administración Local y Ordenación del Territorio* of the Comunidad de Madrid. Mice and samples were randomly assigned to experimental groups. Data collection was performed in a blinded manner whenever technically feasible.

Creation and maintenance of ibrutinib-resistant pools

Ibrutinib-resistant (IR) pools of ABC-DLBCL cell lines were generated by exposing the cells to increasing doses of ibrutinib (ranging from 10-fold below to 2-fold above the GR_{50}) weekly for five weeks, following the protocol described in[20]. These cells were then maintained for an additional two weeks in medium containing ibrutinib at a concentration

2-fold above the GR_{50}. The resulting populations were designated as IR pools. Growth rate inhibition was assessed by culturing cells in medium containing serial dilutions of ibrutinib (Selleck Chem), ranging from 1 nmol/L to 50 µmol/L, depending on the cell line. Viability was measured three days post-treatment using the CellTiter-Glo® reagent. GR_{50} values for the cell lines were as follows: Riva, 50 nM; HBL1, 10 nM; U2932, 10 µM; and MD-901, 18 µM. Prior to performing xenograft experiments in mice, resistance to ibrutinib was confirmed by maintaining the IR pools for two additional weeks in culture: the first week with ibrutinib at the GR_{50} concentration, and the second week with ibrutinib at 2-fold above the GR_{50}.

Lentiviral expression constructs and transductions

Lentiviral pTRIPZ constructs were previously generated in our laboratory[29]. The miR-28 precursor sequence was cloned into a puromycin-resistant, doxycycline-inducible pTRIPZ vector containing an RFP reporter (Thermo Scientific). Lentivirus-containing supernatants were harvested 48 hours after transfection of 293T cells with packaging vectors (VSVG, Δ9.8) and the lentiviral construct plasmids. A scramble (scr)-pTRIPZ vector was used as a control. Transduced human lymphoma cell lines were selected by culturing in the presence of 0.4 µg/ml puromycin for 72 hours. Expression of either miR-28 or the scr sequence was induced by exposure to 0.5 µg/ml doxycycline for 48 hours. Transduced RFP^+ cells were isolated using a FACSAria cell sorter for subsequent experiments. Lentiviral Gene Ontology (LeGO) vectors LeGO-V2 (Venus) and LeGO-Cer2 (Cerulean)[30] were used as color-based tracking vectors. These vectors were used to perform the cell competition assay and the clonal monitoring assay for the generation of ibrutinib resistance.

Apoptosis assays

IR and parental U2932 cells were plated at 200,000 cells/ml and treated with the indicated concentrations of ibrutinib in culture medium. After 72 hours, apoptosis was analyzed by flow cytometry using DAPI and APC Annexin V staining (BioLegend, Cat# 640932).

Cell competition assays

Human ABC-DLBCL cells (HBL1, MD-901, U2932, and Riva) transduced with pTRIPZ-miR-28 or pTRIPZ-scr were further transduced with LeGO lentiviral vectors encoding Cerulean or Venus, respectively. To account for potential color-specific effects, pTRIPZ-scr cells were also transduced with Cerulean. Transduced Cerulean$^+$ and Venus$^+$ cells were isolated by fluorescence-activated cell sorting (FACS) using a FACSAria cell sorter. For each independent well of each cell line, a total of 20,000 cells were seeded at a 1:1 ratio of pTRIPZ-scr-Venus to pTRIPZ-miR-28-Cerulean in 96-well plates, in the presence of ibrutinib (Selleck Chem). Cells were treated weekly with increasing doses of ibrutinib (ranging from 10-fold below to 2-fold above the GR_{50}) to generate ibrutinib-resistant cells, following the protocol described by Shaffer and collaborators[20]. miRNA expression was induced with doxycycline (0.5 µg/mL), and cell cultures were maintained by passaging twice per week in fresh medium supplemented with doxycycline and the corresponding doses of ibrutinib. The percentages of Cerulean$^+$ and Venus$^+$ cells were monitored weekly over five weeks using an LSRFortessa High-Parameter Flow Cytometer and analyzed with FlowJo v10.4.2 software.

Cell Viability

The number of viable cells was determined in MD-901, U2932, HBL1, and Riva DLBCL cells transduced with either scr or miR-28, five weeks after initiating treatment with increasing doses of ibrutinib (ranging from 10-fold below to 2-fold above the GR_{50}), using the CellTiter-Glo® reagent. The same culture dilutions were applied to both scr and miR-

28 transduced cultures throughout the experiment. Luminescence was measured using an Orion Plate Luminometer Reader (Berthold). Relative luminescence units (RLU) were calculated by subtracting background luminescence from wells containing only medium. Data were normalized to control cells treated with ibrutinib only.

Clonal monitoring of ibrutinib resistance generation

Clonal selection during the development of ibrutinib resistance was assessed using MD-901 ABC-DLBCL cells labeled with combinations of LeGO lentiviral vectors encoding Cerulean and Venus fluorescent proteins, adapting a previously described clonal tracking system[31]. Ten labeled cells were seeded per well in 96-well plates (45 independent wells per condition and experiment) and cultured for 5 weeks with weekly increasing doses of ibrutinib (from 10-fold below to 2-fold above the GR_{50}), following established protocols to promote ibrutinib resistance[20]. This assay was performed in two settings: (i) with multicolor-labeled (MCL) MD-901 cells alone, and (ii) with MCL cells additionally transduced with either pTRIPZ-scr or pTRIPZ-miR-28 constructs. In the latter case, miRNA expression was induced by adding 0.5 µg/mL doxycycline. In all conditions, cultures were passaged twice per week in fresh medium supplemented with the corresponding concentrations of ibrutinib and doxycycline as appropriate. Clonal composition was monitored weekly using an LSRFortessa Flow Cytometer based on Cerulean and/or Venus fluorescence. Data were analyzed with FlowJo v10.4.2 software. Clonal evolution was quantified by calculating the fold-change in clone frequency and the Shannon diversity index, relative to baseline (week 1). Wells with two or fewer quantifiable clones were excluded from the analysis.

Mitochondrial Mass

Mitochondrial mass was measured in HBL1, MD-901, and Riva ABC-DLBCL cells transduced with either pTRIPZ-scr or pTRIPZ-miR-28 and treated weekly with increasing doses of ibrutinib (ranging from 10-fold below to 2.5-fold below the GR_{50}) for three weeks. Cells were stained with MitoTracker Green (20–50 nM; Thermo Fisher Scientific) by incubation for 30 minutes at 37 °C in staining medium consisting of RPMI supplemented with 10% fetal bovine serum, 1% penicillin/streptomycin, and 10 mM HEPES (Gibco).

Cellular metabolic activity

Oxygen consumption rate (OCR) and extracellular acidification rate (ECAR) were measured on MD-901 ABC-DLBCL cells previously transduced with either pTRIPZ-scr or pTRIPZ-miR-28 and exposed to increasing doses of ibrutinib (ranging from 10-fold below to 2.5-fold above the GR_{50}) for 3 weeks. Cells were resuspended in Seahorse XF Base Medium (pH 7.4) supplemented with 11 mM glucose and 2 mM pyruvate, and 1×10^6 cells were seeded into 96-well Seahorse assay plates (Seahorse Bioscience) pre-coated with Cell-Tak (Corning). OCR and ECAR were then assessed using the XF96 Extracellular Flux Analyzer and the Seahorse XF Cell Mito Stress Test Kit, following the manufacturer's instructions.

RNA sequencing

Bulk RNA sequencing was performed on the following MD-901 multicolor-labeled (MCL) clones after three weeks of exposure to gradually increasing doses of ibrutinib (ranging from 10-fold below to 2.5-fold above the GR_{50}): ibrutinib-sensitive (scr week 5 < week 1, n = 4), ibrutinib-resistant (scr week 5 > week 1, n = 4), and miR-28–expressing (n = 5). At week 3, RFP^+ cells were isolated by FACS using a FACS Aria cell sorter for RNA extraction and sequencing. Total RNA was extracted from sorted cells using the

miRNeasy Mini Kit (Qiagen) following the manufacturer's protocol. RNA integrity and size distribution were assessed with a Bioanalyzer. Poly(A)+ RNA was enriched using poly-T oligo-attached magnetic beads, followed by fragmentation, cDNA synthesis, end repair, adaptor ligation, uracil excision, and PCR amplification. Barcoded libraries were sequenced on a DNBSEQ platform, and FASTQ files were generated locally at BGI Shenzhen for downstream analysis.

Pathway enrichment analysis

Comparative pathway enrichment analysis was performed using Ingenuity Pathway Analysis (IPA) software[32] to identify signaling networks modulated during the acquisition of ibrutinib resistance and to assess the regulatory impact of miR-28 with the following differential expression analysis MCL clones (using an adjusted p-value threshold of < 0.05): ibrutinib-sensitive clones, ibrutinib-resistant clones, and miR-28–expressing clones, all exposed to increasing doses of ibrutinib for three weeks (w3). Additionally, we used a subset of 265 genes shared between scramble ibrutinib-resistant and ibrutinib-sensitive clones, as well as between miR-28–expressing and scramble ibrutinib-resistant clones at week 3, defined as the miR-28–regulated ibrutinib resistance gene signature. Enriched pathways were filtered using a significance threshold of $-\log_{10}$ (Benjamini-Hochberg p-value) > 2. Pathway activity predictions were based on IPA Z-scores, with positive values indicating predicted activation and negative values indicating inhibition. All p-values were corrected for multiple testing using the Benjamini–Hochberg false discovery rate (FDR).

Gene set enrichment analysis and gene signature analysis

Gene set enrichment analysis (GSEA) was performed to identify signaling pathways regulated by miR-28 during the development of ibrutinib resistance in ABC-DLBCL. GSEA was carried out using RNA sequencing data from: ibrutinib-sensitive clones, ibrutinib-resistant clones, and miR-28–expressing clones, all exposed to increasing doses of ibrutinib for three weeks. Additionally, we used available RNA-seq datasets from ibrutinib-resistant cell lines (OCI-Ly1 IR, OCI-Ly10 IR, and HBL1 IR)[33]. Analysis was conducted using the GSEA software package (Broad Institute), and enrichment was evaluated based on the normalized enrichment score (NES) and false discovery rate (FDR)–adjusted p-values. Reference gene sets used included: BTK inhibitor resistance–associated genes identified by CRISPR-Cas9 screening in ABC-DLBCL cell lines[21], mitochondrial gene sets from MitoCarta 3.0, and the "Hallmark mTORC1 signaling" gene set from curated collections of The Molecular Signatures Database (MSigDB).

Data from the non-China cohort of the PHOENIX trial—study of the Bruton's tyrosine kinase inhibitor, PCI-32765 (Ibrutinib), in combination with rituximab, cyclophosphamide, doxorubicin, vincristine, and prednisone in patients with newly diagnosed Non–Germinal Center B-cell subtype of Diffuse Large B-Cell Lymphoma—used in this study are available through the European Genome-phenome Archive (EGA) at the European Bioinformatics Institute under accession number EGAS00001005554 (dataset EGAD00001008131)[12]. We acknowledge Janssen and Dr. Srimathi Srinivasan for providing access to the data. All analyses and results derived from these data were conducted with the approval of the Data Access Committee (DAC) from Janssen, in accordance with the agreement established with the Spanish National Center for Cardiovascular Research, Madrid, Spain. We applied the *singscore* method to compute a per-sample score reflecting the expression of genes upregulated in the miR-28–regulated ibrutinib resistance program (logFC $\geq$ 1). These scores were then used in survival

analyses to assess their association with patient outcomes. *Singscore* was computed for each patient and used to stratify them into "High" or "Low" groups based on the median value. Overall survival (OS) was analyzed using Kaplan–Meier estimates and the log-rank test, implemented via the survival and survminer R packages. Survival curves were plotted using the ggsurvplot function.

Lymphoma models

For subcutaneous xenografts, a suspension of 1–5 × 10^6 ABC-DLBCL cells was prepared in 100 µL of phosphate-buffered saline (PBS), mixed 1:1 with Matrigel (BD Biosciences), and injected into the flanks of 10–12-week-old NSG mice. The ABC-DLBCL models used included parental or IR MD-901, U2932, and Riva cells, as well as Riva cells transduced with either pTRIPZ-scr-Venus or pTRIPZ-miR-28-Cerulean. Only the transduced Riva cells were cultured for three weeks with gradually increasing doses of ibrutinib (up to 2.5-fold below the GR_{50}) in the presence of doxycycline (Sigma-Aldrich), and subsequently sorted as RFP^+ prior to xenografting. In ibrutinib-treated mice, animals were administered ibrutinib daily via oral gavage at a dose of 20 mg/kg (PCI-32765; MedChemExpress), dissolved in a vehicle consisting of 5% DMSO, 30% polyethylene glycol 300, 5% Tween-80, and 60% water. Control groups received the vehicle alone. When indicated, doxycycline was administered in the drinking water at a concentration of 0.04%, twice weekly. Subcutaneous tumor volume was measured using a digital caliper and calculated with the following formula: volume = $(\text{width})^2 \times \text{length} / 2$.

Treatment with miR-28 mimics

Synthetic miRNA of miR-28 (miR-28 mimics) and the scramble control sequence were obtained from Ambion. Established U2932 IR DLBCL tumors (>150 mm^3) were treated

with weekly intratumor injections of 0.5 nmol miRNA mimics (miR-28 or control) together administered with invivofectamine (Ambion).

Synthesis of miR-28– and aptamer–conjugated gold nanoparticles

Spherical Gold Nanoparticles (AuNP) were synthesized following the Turkevich method in collaboration with Dr. Alvaro Somoza's group. Rounded 11 nm of citrate-covered AuNPs at 33.8 nM were obtained, and the resulting solution was filtered through a 2 µm membrane. miRNA mimics and aptamers were synthesized via phosphoramidite chemistry using a K&A H6/H8 DNA/RNA synthesizer, with 3'-Thiol C6 CPG and rG(dmf) CPG supports for the sense and antisense strands, respectively. Oligonucleotides were purified using MicroPure II affinity columns and annealed by heating a 1:1 mixture of complementary strands at 95 °C for 5 minutes, followed by gradual cooling (1 °C/min) to 4 °C to form duplexes. AuNP functionalization was performed via thiol-gold conjugation using the salt-aging method. Briefly, 8 nmol of miRNA duplex and 2 nmol of aptamer were incubated with a 50-fold excess of 0.5 M TCEP for 1 h to reduce disulfide bonds. The reduced oligonucleotides were added to 16 nM citrate-stabilized AuNPs and incubated for 2 h. NaCl (5 M) was then added stepwise to reach a final concentration of 0.5 M, followed by overnight incubation under stirring. Functionalized AuNPs were purified by centrifugation (15,000 ×g, 1 h, 3 cycles) to remove unbound oligonucleotides. Oligonucleotide loading was quantified indirectly by measuring the absorbance at 260 nm of the first supernatant. The sequences used were: 5'-rCrArArUrArGrArCrUrGrUrGrArGrCrUrCrCrUrUTTAAA-C6Thiol-3' for miRNA-28 sense, 5'-rArArGrGrArGrCrUrCrArCrArGrUrCrUrArUrUrGrArG-3' for miRNA-28 antisense, 5'-TTCGCTCTCCCTTACGGGCTTACATGTTCGCATCCCCCCTT-C6Thiol-3' for CD19 aptamer[34], 5'-TTCGCCCTCTGTTTCTGCCTTATTATTTTTGTTTGCTTCT-C6Thiol-3' for CD20

aptamer[34]. The scramble miRNA sequence employed was 5'-rArArGrGrCrCrArGrArCrGrCrGrArArUrUrArUTTTTT-C6Thiol-3' for sense, 5'-rArUrArArUrUrCrGrCrGrUrCrUrGrGrCrCrUrU -3' for the antisense strand.

Treatment with aptamer-conjugated AuNP-miR-28

miR-28- or scr-functionalized nanoparticles conjugated with CD19 or CD20 aptamers were used to treat established IR ABC-DLBCL tumors (>150 mm^3). Tumors were treated twice weekly with 2.3 pmol intratumoral injections of nanoparticles, containing either miR-28 or the control sequence.

Flow Cytometry

Flow cytometry analyses were performed at the Flow Cytometry Core Facility (Centro de Apoyo a la Investigación, CAI) of the Universidad Complutense de Madrid and at the Flow Cytometry Facility of the Centro Nacional de Investigaciones Cardiovasculares (CNIC). Samples were acquired using BD Celesta™, BD Fortessa™, and BD FACSymphony™ cytometers, and cell sorting was performed using BD FACSAria™ II and BD FACSAria™ Fusion cell sorters.

Statistics and figures

Sample sizes were selected to ensure confidence in the results and measurements, based on prior studies. The number of mice used in each experiment is indicated in the figure legends and/or the Methods section. Statistical analyses were performed using GraphPad Prism 8 and are specified in the figure legends. Error bars represent either the standard deviation or the standard error of the mean (SEM), as indicated. Data normality was assessed using the Anderson-Darling test. Normally distributed data were analyzed using a two-tailed unpaired Student's t-test for comparisons between two groups, or ANOVA

for comparisons among more than two groups. Differences were considered statistically significant at $p < 0.05$. The graphical abstract was created using Biorender.

RESULTS

miR-28 inhibits the generation of ibrutinib resistance in ABC-DLBCL cells

To evaluate the impact of miR-28 on the development of ibrutinib resistance in ABC-DLBCL, we first established a polyclonal competition assay using flow cytometry and assessed the effect of miR-28 in four human ABC-DLBCL cell lines: MD-901, U2932, Riva, and HBL1. In this assay, we mixed, in a 1:1 ratio, populations of each ABC-DLBCL cell line transduced with pTRIPZ doxycycline-inducible lentiviral vectors encoding either miR-28 or a scramble (scr) sequence, along with RFP[29]. The pTRIPZ-transduced ABC-DLBCL cells used in the assay were additionally labeled by transduction with vectors encoding fluorescent proteins, Cerulean for miR-28-transduced cells and Venus for scr-transduced cells (Figure 1A). The mixed miR-28-Cerulean and scr-Venus populations were cultured for five weeks in the presence of doxycycline and exposed to ibrutinib at concentrations that increased weekly from approximately 10-fold below to approximately 2-fold above the ibrutinib growth rate inhibition 50% value (GR_{50}), a process that leads to the generation of ibrutinib-resistant ABC-DLBCL cells[20](Figure S1A). The cultures were analyzed weekly by flow cytometry to quantify changes in the relative proportions of miR-28-Cerulean and scr-Venus cells (Figure 1A-B). We found that the proportion of RFP^+ miR-28-$Cerulean^+$ cells in the four ABC-DLBCL cell lines gradually decreased as ibrutinib concentrations increased, and that the contribution of miR-28-expressing cells in ibrutinib-resistant cultures (week 5) was significantly lower than in the starting cultures (Figure 1B-C, S2A). RFP^+ miR-28-$Cerulean^+$ cells accounted for a minor proportion of the cells (18% of U2932, and ≤ 9% of MD-901, Riva and HBL1) after five weeks of culture in the presence of ibrutinib (Figure S1B). To exclude any possible effect of Cerulean and Venus fluorescent protein expression on the competition assay, we also

performed a control competition assay in scr-transduced MD-901 ABC-DLBCL cells. As expected, we found no significant differences in the proportions of scr-Cerulean and scr-Venus populations after five weeks of culture with increasing ibrutinib concentrations (Figure 1D, S1C). In agreement with the previous results, we found that the generation of ibrutinib-resistant cells was diminished in MD-901, U2932, and HBL1 ABC DLBCL cells expressing miR-28 (Figure S1D), and that miR-28 pTRIPZ-transduced Riva ABC DLBCL cell cultures were enriched in RFP^- cells by the time when ibrutinib-resistant generation had occurred (week 5) (Figure S1E). Together, these results show that miR-28 inhibits the generation of ibrutinib-resistant ABC-DLBCL cells.

miR-28 inhibits clonal selection during ibrutinib resistance generation in ABC-DLBCL cells

To determine whether miR-28 limits the generation of ibrutinib-resistant cells solely by impairing proliferation or promoting cell death, or whether it can actively suppress the development of resistance, we developed a flow cytometry–based assay to analyze resistance emergence at the clonal level using MD-901 cells. To monitor clonal diversity, we first generated a multicolor-labeled (MCL) ABC-DLBCL cell population by transducing MD-901 cells with lentiviral vectors encoding Venus and Cerulean fluorescent proteins. Ten MCL cells, each expressing a random number of Venus and/or Cerulean-encoding lentiviral copies, were seeded into 96-well plates. These fluorescently barcoded cells were then treated for five weeks with ibrutinib at concentrations that increased weekly from 10-fold below to 2-fold above the GR_{50} in MD-901 cells, or were left untreated (n = 45 wells per condition). The proportions of the different MCL clones in each well were monitored weekly by flow cytometry to quantify changes over time. We found that the gradual increase in ibrutinib concentration led to the selection of a

subset of clones—approximately 25%—within each well, whereas the proportions of clones in untreated wells remained more stable over time (Figure 2A-B, S2E-F). Accordingly, the diversity index of ibrutinib-treated wells was reduced over time compared to untreated wells (Figure 2C-D). Thus, we conclude that the MCL assay enables monitoring of clonal selection and the emergence of ibrutinib-resistant clones that outcompete ibrutinib-sensitive cells during the development of resistance in ABC-DLBCL cells.

Next, we used the MCL clonal assay to test the effect of miR-28 expression on the generation of ibrutinib resistance. We found that miR-28 expression impaired the emergence of ibrutinib-resistant clones, as the proportions of MCL clones remained more stable during the first three weeks of culture, with gradually increasing ibrutinib doses, in wells seeded with miR-28-expressing MCL cells compared to those seeded with cells expressing a scramble construct (Figure 3A-B). Accordingly, the diversity index of miR-28 MCL wells was higher than that of scramble MCL wells (Figure 3C).

After five weeks of culture, when ibrutinib concentration is 2-fold above the MD-901 GR_{50}, we found that scramble MCL wells reached a high cellular density, whereas wells containing miR-28 MCL cells were more heterogeneous in cell density and included medium and low cellular densities (Figure S2B). RFP expression analysis revealed that wells with low cellular density had a higher percentage of RFP^+ cells than medium-density miR-28 MCL wells (Figure 4A). Moreover, t-SNE analysis of RFP expression showed that miR-28 RFP^+ MCL cells present at week 1 were preferentially depleted at week 5 in medium-density wells, but not in low-density wells (Figure 4B). Given that miR-28 expression correlates with RFP expression (Figure S2C), these results suggest an inverse correlation between RFP expression and cell survival of miR-28–expressing cells in gradually increasing ibrutinib cultures. To determine whether there is a correlation

between RFP expression and the generation of ibrutinib-resistant cells in miR-28 MCL wells, we quantified the RFP mean fluorescent intensity of all the MCL clones (655 miR-28 MCL clones and 617 scr MCL clones), analyzing them according to their relative increase or decrease in proportions in week 5 (w5) *versus* week 1 (w1) cultures. We found that RFP expression was higher in miR-28 MCL clones that were counter-selected in the presence of ibrutinib (w5 < w1), but did not change in scramble MCL clones regardless of whether the clones had become resistant to ibrutinib (w5 > w1) or were ibrutinib-sensitive (w5 < w1) (Figure 4C). In addition, we quantified the number of ibrutinib-resistant cells generated in scramble and miR-28 MCL wells. We found a reduced number of viable MCL cells after five weeks of culture with increasing ibrutinib concentrations in miR-28 wells (Figure 4D, S2D). Together, these results show that miR-28 impairs the generation of ibrutinib-resistant ABC-DLBCL cells.

miR-28 inhibits signaling pathways required for the development of ibrutinib resistance in ABC-DLBCL

To identify miR-28–regulated signaling pathways involved in the acquisition of ibrutinib resistance, we performed RNA transcriptomic analysis after three weeks of culture with gradually increasing doses of ibrutinib, prior to the full establishment of resistance. We analyzed scramble ibrutinib-sensitive clones (defined as week 5 < week 1), scramble ibrutinib-resistant clones (defined as week 5 > week 1), and miR-28–expressing MCL clones (Figure S3A). Principal component analysis (PCA) of transcriptomic profiles revealed clustering by condition, with high intra-group similarity across the three experimental groups (Figure 5A). RNA-seq analysis comparing ibrutinib-sensitive (n = 4) and week 3–resistant scramble (n = 4) MCL clones identified 695 differentially expressed genes (DEG) associated with resistance development. Transcriptomic

comparison between miR-28–expressing clones (n = 5) and week 3–resistant (n = 4) MCL clones revealed miR-28–dependent modulation of 3,370 transcripts (Table S1). Notably, Gene Set Enrichment Analysis (GSEA) showed that week 3–resistant MCL clones upregulated the expression of genes previously found to be essential for BTK-inhibitor resistance in HBL1, OCI-Ly10 and TMD8 ABC-DLBCL cells using a genome-wide CRISPR-Cas9 screen[21] ($p = 0.003$, NES = 1.42) (Figure 5B). In contrast, the expression of these resistance-associated genes was significantly downregulated in miR-28–expressing MCL clones ($p \leq 0.000$, NES = –2.21) (Figure 5B). Ingenuity Pathway Analysis (IPA) further revealed that resistance acquisition in scramble MCL clones is linked to downregulation of gene networks involved in cellular stress responses (e.g., eIF2 signaling, nonsense-mediated decay, amino acid deficiency response, ribosomal quality control) and different metabolic processes (e.g., translation, selenoamino acid metabolism, oxidative phosphorylation). Conversely, upregulation of mTOR and mitochondrial signaling was observed in week 3–ibrutinib resistant MCL clones (Figure S3B, Table S2). In miR-28–expressing MCL clones, these pathway alterations were reversed, with activation of stress and metabolic programs and suppression of mTOR and mitochondrial signaling (Figure S3B, Table S2). Consistently, GSEA using MitoCarta 3.0[35] confirmed that mitochondrial pathway expression was downregulated in miR-28–expressing MCL clones and upregulated in ibrutinib-resistant MCL clones following three weeks of ibrutinib exposure (Figure 5C). Consistent with these findings, analysis of publicly available datasets from ibrutinib-resistant HBL1, OCI-Ly10, and OCI-Ly1 models[33] also revealed upregulation of mitochondrial-related pathways linked to ibrutinib resistance (Figure S3C).

Next, we analyzed the specific set of genes involved in the acquisition of ibrutinib resistance that are regulated by miR-28 in MCL MD-901 clones, by comparing DEGs

between scramble ibrutinib-resistant and ibrutinib-sensitive clones, as well as between miR-28–expressing and scramble ibrutinib-resistant clones at week 3. We found that miR-28 regulates 265 of the 695 DEGs associated with resistance development (Figure 5D). Hierarchical clustering of MCL clones based on the expression of these 265 genes showed that miR-28–expressing MCL clones clustered with ibrutinib-sensitive clones, but not with week 3–resistant clones. This clustering pattern reflects the coordinated regulation of this gene subset shared between miR-28–expressing and ibrutinib-sensitive clones, which is associated with the suppression of mTOR (Figure 5D, S3B, Table S2). We refer to this subset as the miR-28–regulated ibrutinib-resistance (miR-28-IR) gene signature. Given these transcriptomic findings, which reveal changes in cellular metabolism pathways related to mitochondrial biogenesis, we next assessed the mitochondrial status of scramble and miR-28–expressing ABC-DLBCL cells after three weeks of culture in the presence of gradually increasing doses of ibrutinib. MitoTracker Green staining and flow cytometry revealed reduced mitochondrial mass in miR-28–expressing MD-901, Riva, and HBL1 cells compared to scramble controls (Figure 5E). Seahorse analysis further showed that, although oxygen consumption rate (OCR) and extracellular acidification rate (ECAR) were similar between groups, miR-28–expressing MD-901 cells exhibited lower mitochondria-derived ATP production (Figure S3D). To evaluate mTOR activity, we measured phosphorylation of ribosomal protein S6 (pS6) by flow cytometry. pS6 levels were consistently lower in miR-28–expressing MD-901, Riva, and HBL1 cells after three weeks of ibrutinib exposure (Figure 5F). Consistent with these findings, miR-28 downregulated mTOR pathway genes in MD-901 cells that are also upregulated in ibrutinib-resistant ABC-DLBCL cell lines such as OCI-Ly1, OCI-Ly10, and HBL1[33] (Figure S3E). Overall, these findings show that miR-28 counteracts both

mitochondrial and mTOR signaling adaptations associated with the development of ibrutinib resistance in ABC-DLBCL cells.

Survival of ibrutinib-treated MCD DLBCL patients is associated with the miR-28–regulated ibrutinib resistance gene signature

To assess whether the transcriptional program induced by miR-28 in ibrutinib-treated ABC-DLBCL cells is associated with differences in survival among DLBCL patients, we analyzed outcome data from patients with the MCD (73), BN2 (31), and N1 (24) genetic subtypes of DLBCL who were treated with R-CHOP immunochemotherapy or R-CHOP plus ibrutinib and had five years of outcome data[12]. Patients were ranked based on a singscore analysis[36] of the expression of genes associated with ibrutinib resistance from the miR-28-IR gene signature (logFC > 1), using baseline biopsies from the non-GCB DLBCL PHOENIX trial. Singscore is a method that assigns a score to each sample based on the relative expression of genes in a predefined signature, enabling comparison of signature activity across patients. Patients were then stratified into two groups (high and low score) according to the median score. Correlation with clinical outcomes revealed that MCD patients—the most prevalent genetic subtype related to ABC-DLBCL—with low singscore had higher overall survival than those with higher singscore when treated with ibrutinib, but not when treated with R-CHOP alone. However, this difference was statistically significant only in older MCD patients (age > 60 years; n = 54, p = 0.047) (Figure 5G, S3F). No significant differences in survival between patients with low and high singscore rankings were observed in N1 or BN2 DLBCL subtypes, regardless of ibrutinib treatment (data not shown). Thus, we identified a set of genes specifically downregulated by miR-28 as important determinants of survival in ibrutinib-treated MCD DLBCL patients.

miR-28 suppresses the emergence and growth of ibrutinib-resistant ABC-DLBCL tumors

To evaluate the anti-tumor activity of miR-28 in ibrutinib-resistant B-cell lymphoma, we used different models of ABC-DLBCL with acquired resistance to ibrutinib. We first assessed the growth capacity of parental and ibrutinib-resistant U2932, MD-901, and Riva ABC-DLBCL cell lines, and found that the resistant cells exhibited enhanced growth in xenograft tumor models (Figure 6A). Next, we investigated whether miR-28 expression could inhibit the development of ibrutinib-resistant tumors in human ABC-DLBCL xenografts. Riva cells transduced with either scramble or miR-28-pTRIPZ constructs and Venus or Cerulean proteins were co-cultured *in vitro* for three weeks in the presence of doxycycline and progressively increasing concentrations of ibrutinib (ranging from 10-fold below to 2.5-fold below the GR_{50}). After this period, RFP^+ miR-28-$Cerulean^+$ and RFP^+ scr-$Venus^+$ cells were sorted by flow cytometry and injected subcutaneously into NOD scid gamma (NSG) mice. The animals received doxycycline in their drinking water and daily doses of vehicle or 20 mg/kg ibrutinib, a dose that, as shown in our results, effectively inhibits parental Riva xenograft growth (Figure S4A). Scramble tumors in ibrutinib-treated mice were larger than those in vehicle-treated controls, indicating the emergence of *in vivo* ibrutinib resistance (Figure 6B). Notably, in ibrutinib-treated groups, xenografts with induced miR-28 expression exhibited significantly reduced tumor volumes compared to scramble controls (Figure 6B). These findings demonstrate that miR-28 inhibits the development of ibrutinib-resistant ABC-DLBCL tumors in xenografts.

We further evaluated the therapeutic potential of miR-28 analogs delivered via different methods *in vivo* in models of ibrutinib-resistant ABC-DLBCL. First, ibrutinib-resistant U2932 ABC-DLBCL tumors were treated with synthetic miR-28 mimics or scramble controls. Once tumors reached at least 150 mm^3, mice received intratumoral injections of 0.5 nmol of either miR-28 or control mimics. Treatment with miR-28 significantly

inhibited the growth of ibrutinib-resistant U2932 tumors (Figure 6C). Notably, the inhibitory effect of miR-28 was stronger in ibrutinib-resistant tumors than in those derived from parental U2932 cells (2.1-fold reduction after one treatment vs. 1.3-fold reduction after three treatments, respectively; Figure 6C). Finally, we assessed whether aptamer-conjugated, lymphoma-targeted AuNPs carrying miR-28 could inhibit tumor growth. Ibrutinib-resistant ABC-DLBCL cell lines (U2932, MD-901, and Riva) were subcutaneously injected into NSG mice. After the tumors reached at least 150 mm^3, mice were treated with intratumoral injections of control or miR-28 AuNPs conjugated to CD19- or CD20-specific aptamers. The xenografted cell lines expressed distinct surface markers (MD-901: $CD19^+CD20^-$; U2932: $CD19^{low}CD20^+$; Riva: $CD19^+CD20^+$; Figure S4B). Treatment of ibrutinib-resistant MD-901 tumors with CD19-targeted miR-28 AuNPs significantly inhibited tumor growth (Figure 6D, S4C-D). This antitumor effect was specific to miR-28 and the aptamer-targeted delivery, as the inhibition was observed compared to CD20-targeted miR-28 AuNPs or control AuNPs. Similar results were observed in ibrutinib-resistant U2932 and Riva xenografts treated with aptamer-conjugated miR-28 AuNPs targeting their respective surface markers (Figure 6D). Our findings demonstrate that ibrutinib-resistant tumors retain sensitivity to miR-28-mediated inhibition. Targeted delivery via aptamer-conjugated gold nanoparticles enables this effect *in vivo*, underscoring the translational potential of miR-28 as a therapeutic strategy to counter resistance in ABC-DLBCL.

DISCUSSION

In spite of the major advances in the identification of molecular drivers in DLBCL, a significant subset of these aggressive B-cell lymphomas remains a major clinical challenge[3, 4]. Although ABC-DLBCL initially responds to BTK inhibitor–based targeted therapies, the emergence of acquired resistance continues to limit durable clinical benefit[10, 14, 19]. In this study, we investigated whether the microRNA miR-28 could impair the development of non-genetic resistance to ibrutinib in ABC-DLBCL. We hypothesized that the activity of miR-28, which simultaneously inhibits the expression of several genes identified as essential for oncogenic signaling—including genes from the BCR-dependent PI3K and NF-κB pathways[29]— could disrupt the feedback activation and transcriptional rewiring associated with resistance.

Using a combination of flow cytometry–based competition assays, clonal barcoding with multicolor labeling, transcriptomic profiling, and *in vivo* xenograft models, we show that miR-28 impairs the emergence of ibrutinib-resistant cells in ABC-DLBCL. These results build upon seminal work identifying the transcriptional remodeling associated with the development of ibrutinib resistance in ABC-DLBCL, as well as the genes essential for the survival of resistant cells, as revealed by genome-wide CRISPR-Cas9 screens[20, 21]. In ibrutinib-exposed MD-901 clones, miR-28 downregulated genes previously shown to be critical for resistance acquisition in HBL1, OCI-Ly10, and TMD8 ABC-DLBCL cells[21]. Pathway analysis of these clones further revealed that miR-28 suppresses the upregulation of mTOR and mitochondrial signaling—responses specifically induced after three weeks of adaptation to increasing ibrutinib doses. These observations are consistent with previous reports implicating PI3K/AKT/mTOR pathway activation in other ibrutinib- and PI3Kβ/δ inhibitor-resistant ABC-DLBCL models[20, 33, 37]. Moreover, our reanalysis of

publicly available datasets from resistant models[33] confirmed the enrichment of mitochondrial-related pathways, including those linked to resistance in HBL1, OCI-Ly10, and OCI-Ly1 cell lines. To support these findings, we assessed mTOR activity and mitochondrial function—such as ATP production rate and mitochondrial mass—in three ABC-DLBCL cell lines exposed to increasing ibrutinib concentrations, with or without miR-28 expression. These results confirmed the capacity of miR-28 to modulate key transcriptomic and metabolic changes associated with resistance development.

Reinforcing the functional relevance of these transcriptomic alterations, we found that the expression of resistance-associated genes downregulated by miR-28—comprising the miR-28-IR signature—correlates with survival in ibrutinib-treated MCD-subtype DLBCL patients aged over 60 years in the PHOENIX clinical trial cohort. This clinical correlation is particularly relevant given that MCD and N1—two of the three genetic subtypes related to ABC-DLBCL—are the most responsive to ibrutinib due to their reliance on the BCR–NF-κB signaling pathway, with MCD being substantially more prevalent than N1[12]. Additionally, most ABC-DLBCL cases occur in patients older than 60[12, 38]. Altogether, these findings highlight the potential of miR-28 to target resistance-associated transcriptional programs of clinical relevance.

To investigate how these changes contribute to clonal selection and resistance emergence, we developed a clonal color barcoding flow cytometry–based assay that enabled us to track the fate of individual MD-901 clones during ibrutinib exposure. Approximately one-fourth of the clones became resistant after five weeks of dose escalation, driven by transcriptional adaptations that included the rewiring of metabolism-related pathways and activation of alternative survival signaling. Crucially, miR-28 disrupted this clonal selection process, acting as a brake on the emergence of resistant subpopulations. Beyond

in vitro analyses, we evaluated the development of ibrutinib resistance *in vivo* and demonstrated that miR-28 impairs the growth of ibrutinib-resistant xenografts.

While previous studies have proposed targeting individual proteins within alternative signaling pathways—such as components of the PI3K/AKT axis—to inhibit the growth of ibrutinib-resistant ABC-DLBCL cells or xenograft tumors[33, 39, 40, 41, 42], whether resistance itself can be proactively prevented has remained unaddressed. Here, we demonstrate for the first time that the emergence of resistance in ABC-DLBCL can be actively suppressed—rather than treated only after it is established—using a miRNA-based intervention.

In addition to its preventive effects, we found that rapidly growing ibrutinib-resistant ABC-DLBCL cells remain sensitive to miR-28–mediated inhibition in xenografts. Notably, in our study, this effect was efficiently achieved through targeted delivery using aptamer-guided gold nanoparticles. By using aptamers tailored to each DLBCL cell line, AuNPs enabled efficient tumor targeting and uptake, as shown by the pronounced tumor suppression achieved with AuNP–miR-28–CD19 in MD-901 xenografts compared to non-specific controls. Such aptamer-guided AuNP delivery strategies, which can be administered locally or systemically, not only amplify on-target activity while minimizing exposure in non-malignant tissues, but also protect miR-28 from extracellular degradation and ensure sustained release. These properties highlight the clinical potential of aptamer-functionalized AuNPs as a selective and durable miRNA delivery system[43, 44, 45, 46] for DLBCL treatment. Building on these findings, further studies focusing on: (i) the identification of DLBCL-specific cell surface molecules not expressed in non-malignant B cells and targetable with aptamers, (ii) the development of clinically scalable, tumor-specific miRNA-based drug delivery systems, (iii) the design of optimal miRNA-based combination therapies tailored to ABC-DLBCL patients across different genetic

backgrounds and age groups, and (iv) the validation of these findings in clinical settings, will further enhance the translational potential of this work.

In summary, the results of this study provide insights into the development of targeted miR-28-based therapies delivered via aptamer-functionalized gold nanoparticles to prevent or overcome ibrutinib resistance in ABC-DLBCL.

AUTHOR CONTRIBUTIONS

E.A.C., R.M.P., M.L., T.F.N, B.S.E and S.M. performed experiments. C.G.E. performed computational analysis. M.M. synthesized aptamer- and miRNA-conjugated AuNPs. E.A.C., R.M.P., M.L., T.F.N, B.S.E and V.G.Y. analyzed and interpreted data. E.A.C. prepared figures and wrote Material and Methods. A.S., N.M.M. and A.R.R. contributed to the conception of the experimental design. V.G.Y. conceived the overall strategy and wrote the manuscript. All authors revised and contributed to the final manuscript.

ACKNOWLEDGEMENTS

We thank Janssen and the European Genome-phenome Archive for providing access to data from the PHOENIX trial, the members of the B cell biology lab for helpful discussions, and Arantzazu Alfranca for providing the LeGO vectors. E.A.C. and R.M.P were supported by PhD fellowships from the Comunidad de Madrid (PIPF-2022/SAL-GL-24469 and PIPF-2023/SAL-GL-29484 respectively), A.R.R. by CNIC funding and V.G.Y. by the Universidad Complutense de Madrid. This work was funded by Spanish Ministerio de Ciencia e Innovación grants PID2019-107551RB-I00/AEI/10.13039/501100011033 and PID2022-137014OB-I00/AEI/10.13039/501100011033/ FEDER, UE to V.G.Y and PID2023-146982OB-I00 and CEX2020-001039-S to A.S and IMDEA Nanociencia, respectively. The CNIC is supported by the Instituto de Salud Carlos III (ISCIII), the Ministerio de Ciencia e Innovación (MCIN) and the Pro CNIC Foundation), and is a Severo Ochoa Center of Excellence (grant CEX2020-001041-S funded by MICIN/AEI/10.13039/501100011033).

REFERENCES

1. Susanibar-Adaniya, S. & Barta, S.K. 2021 Update on Diffuse large B cell lymphoma: A review of current data and potential applications on risk stratification and management. *Am J Hematol* **96**, 617-629 (2021).

2. Alizadeh, A.A. *et al.* Distinct types of diffuse large B-cell lymphoma identified by gene expression profiling. *Nature* **403**, 503-511 (2000).

3. Schmitz, R. *et al.* Genetics and Pathogenesis of Diffuse Large B-Cell Lymphoma. *N Engl J Med* **378**, 1396-1407 (2018).

4. Young, R.M. *et al.* Taming the Heterogeneity of Aggressive Lymphomas for Precision Therapy. *Annu Rev Canc Biol* **3**, 429-455 (2019).

5. Davis, R.E. *et al.* Chronic active B-cell-receptor signalling in diffuse large B-cell lymphoma. *Nature* **463**, 88-92 (2010).

6. Reddy, A. *et al.* Genetic and Functional Drivers of Diffuse Large B Cell Lymphoma. *Cell* **171**, 481-494 e415 (2017).

7. Phelan, J.D. *et al.* A multiprotein supercomplex controlling oncogenic signalling in lymphoma. *Nature* **560**, 387-391 (2018).

8. Davis, R.E., Brown, K.D., Siebenlist, U. & Staudt, L.M. Constitutive nuclear factor kappaB activity is required for survival of activated B cell-like diffuse large B cell lymphoma cells. *J Exp Med* **194**, 1861-1874 (2001).

9. Pal Singh, S., Dammeijer, F. & Hendriks, R.W. Role of Bruton's tyrosine kinase in B cells and malignancies. *Mol Cancer* **17**, 57 (2018).

10. Wilson, W.H. *et al.* Targeting B cell receptor signaling with ibrutinib in diffuse large B cell lymphoma. *Nat Med* **21**, 922-926 (2015).

11. Johnson, P.W.M. *et al.* Clinical impact of ibrutinib plus R-CHOP in untreated DLBCL coexpressing BCL2 and MYC in the phase 3 PHOENIX trial. *Blood Adv* **7**, 2008-2017 (2023).

12. Wilson, W.H. *et al.* Effect of ibrutinib with R-CHOP chemotherapy in genetic subtypes of DLBCL. *Cancer Cell* **39**, 1643-1653 e1643 (2021).

13. Younes, A. *et al.* Randomized Phase III Trial of Ibrutinib and Rituximab Plus Cyclophosphamide, Doxorubicin, Vincristine, and Prednisone in Non-Germinal Center B-Cell Diffuse Large B-Cell Lymphoma. *J Clin Oncol* **37**, 1285-1295 (2019).

14. Young, R.M., Phelan, J.D., Wilson, W.H. & Staudt, L.M. Pathogenic B-cell receptor signaling in lymphoid malignancies: New insights to improve treatment. *Immunol Rev* **291**, 190-213 (2019).

15. Jones, D. *et al.* C2 domain mutations co-occur with and resistance mutations in chronic lymphocytic leukemia undergoing ibrutinib treatment. *Leukemia* **31**, 1645-1647 (2017).

16. Woyach, J.A. *et al.* Resistance Mechanisms for the Bruton's Tyrosine Kinase Inhibitor Ibrutinib. *New Engl J Med* **370**, 2286-2294 (2014).

17. Liu, T.M. *et al.* Hypermorphic mutation of phospholipase C, γ2 acquired in ibrutinib-resistant CLL confers BTK independency upon B-cell receptor activation. *Blood* **126**, 61-68 (2015).

18. Wang, E. *et al.* Mechanisms of Resistance to Noncovalent Bruton's Tyrosine Kinase Inhibitors. *New Engl J Med* **386**, 735-743 (2022).

19. Liu, X. *et al.* BTK inhibitors resistance in B cell malignancies: Mechanisms and potential therapeutic strategies. *Blood Rev* **71** (2025).

20. Shaffer, A.L., 3rd *et al.* Overcoming Acquired Epigenetic Resistance to BTK Inhibitors. *Blood Cancer Discov* **2**, 630-647 (2021).

21. Phelan, J.D. *et al.* Response to Bruton's tyrosine kinase inhibitors in aggressive lymphomas linked to chronic selective autophagy. *Cancer Cell* **42**, 238-252 e239 (2024).

22. Ebert, M.S. & Sharp, P.A. Roles for microRNAs in conferring robustness to biological processes. *Cell* **149**, 515-524 (2012).

23. Fuertes, T., Salgado, I. & de Yebenes, V.G. microRNA Fine-Tuning of the Germinal Center Response. *Front Immunol* **12**, 660450 (2021).

24. Fuertes, T., Ramiro, A.R. & de Yebenes, V.G. miRNA-Based Therapies in B Cell Non-Hodgkin Lymphoma. *Trends Immunol* **41**, 932-947 (2020).

25. Rupaimoole, R. & Slack, F.J. MicroRNA therapeutics: towards a new era for the management of cancer and other diseases. *Nat Rev Drug Discov* **16**, 203-222 (2017).

26. Song, J. *et al.* Targeting epigenetic regulators as a promising avenue to overcome cancer therapy resistance. *Signal Transduct Target Ther* **10**, 219 (2025).

27. Schneider, C. *et al.* MicroRNA 28 controls cell proliferation and is down-regulated in B-cell lymphomas. *Proc Natl Acad Sci U S A* **111**, 8185-8190 (2014).

28. Fuertes, T. *et al.* miR-28-based combination therapy impairs aggressive B cell lymphoma growth by rewiring DNA replication. *Cell Death Dis* **14**, 687 (2023).

29. Bartolome-Izquierdo, N. *et al.* miR-28 regulates the germinal center reaction and blocks tumor growth in preclinical models of non-Hodgkin lymphoma. *Blood* **129**, 2408-2419 (2017).

30. Weber, K., Bartsch, U., Stocking, C. & Fehse, B. A multicolor panel of novel lentiviral "gene ontology" (LeGO) vectors for functional gene analysis. *Mol Ther* **16**, 698-706 (2008).

31. Weber, K., Thomaschewski, M., Benten, D., Fehse B. RGB marking with lentiviral vectors for multicolor clonal cell tracking. *Nature Protocols* (2012).

32. Krämer A, G.J., Pollard J Jr, Tugendreich S. Causal analysis approaches in Ingenuity Pathway Analysis. *Bioinformatics* (2014).

33. Jain, N. *et al.* Targeting phosphatidylinositol 3 kinase-beta and -delta for Bruton tyrosine kinase resistance in diffuse large B-cell lymphoma. *Blood Adv* **4**, 4382-4392 (2020).

34. Williams, N.B. *et al.* An In Vitro Selection Platform to Identify Multiple Aptamers against Multiple Cell-Surface Markers Using Ligand-Guided Selection. *Biochemistry* **61**, 1600-1613 (2022).

35. Rath, S. *et al.* MitoCarta3.0: an updated mitochondrial proteome now with sub-organelle localization and pathway annotations. *Nucleic Acids Res* **49**, D1541-D1547 (2021).

36. Foroutan, M. *et al.* Single sample scoring of molecular phenotypes. *BMC Bioinformatics* **19**, 404 (2018).

37. Xu, W. *et al.* mTOR inhibition amplifies the anti-lymphoma effect of PI3Kbeta/delta blockage in diffuse large B-cell lymphoma. *Leukemia* **37**, 178-189 (2023).

38. Mareschal, S. *et al.* The proportion of activated B-cell like subtype among de novo diffuse large B-cell lymphoma increases with age. *Haematologica* **96**, 1888-1890 (2011).

39. Liu, Y. *et al.* EGR1-mediated metabolic reprogramming to oxidative phosphorylation contributes to ibrutinib resistance in B-cell lymphoma. *Blood* **142**, 1879-1894 (2023).

40. Kapoor, I. *et al.* Resistance to BTK inhibition by ibrutinib can be overcome by preventing FOXO3a nuclear export and PI3K/AKT activation in B-cell lymphoid malignancies. *Cell Death Dis* **10**, 924 (2019).

41. Kuo, H.P. *et al.* Combination of Ibrutinib and ABT-199 in Diffuse Large B-Cell Lymphoma and Follicular Lymphoma. *Mol Cancer Ther* **16**, 1246-1256 (2017).

42. Zhang, X.T. *et al.* Activation of unfolded protein response overcomes Ibrutinib resistance in diffuse large B-cell lymphoma. *Acta Pharmacol Sin* **42**, 814-823 (2021).

43. Millozzi, F. *et al.* Aptamer-conjugated gold nanoparticles enable oligonucleotide delivery into muscle stem cells to promote regeneration of dystrophic muscles. *Nat Commun* **16**, 577 (2025).

44. Zhang, R., Kiessling, F., Lammers, T. & Pallares, R.M. Clinical translation of gold nanoparticles. *Drug Deliv Transl Res* **13**, 378-385 (2023).

45. Kumthekar, P. *et al.* A first-in-human phase 0 clinical study of RNA interference-based spherical nucleic acids in patients with recurrent glioblastoma. *Sci Transl Med* **13** (2021).

46. Tao, Z. *et al.* Spherical nucleic acids: emerging amplifiers for therapeutic nanoplatforms. *Nanoscale* **16**, 4392-4406 (2024).

Figures

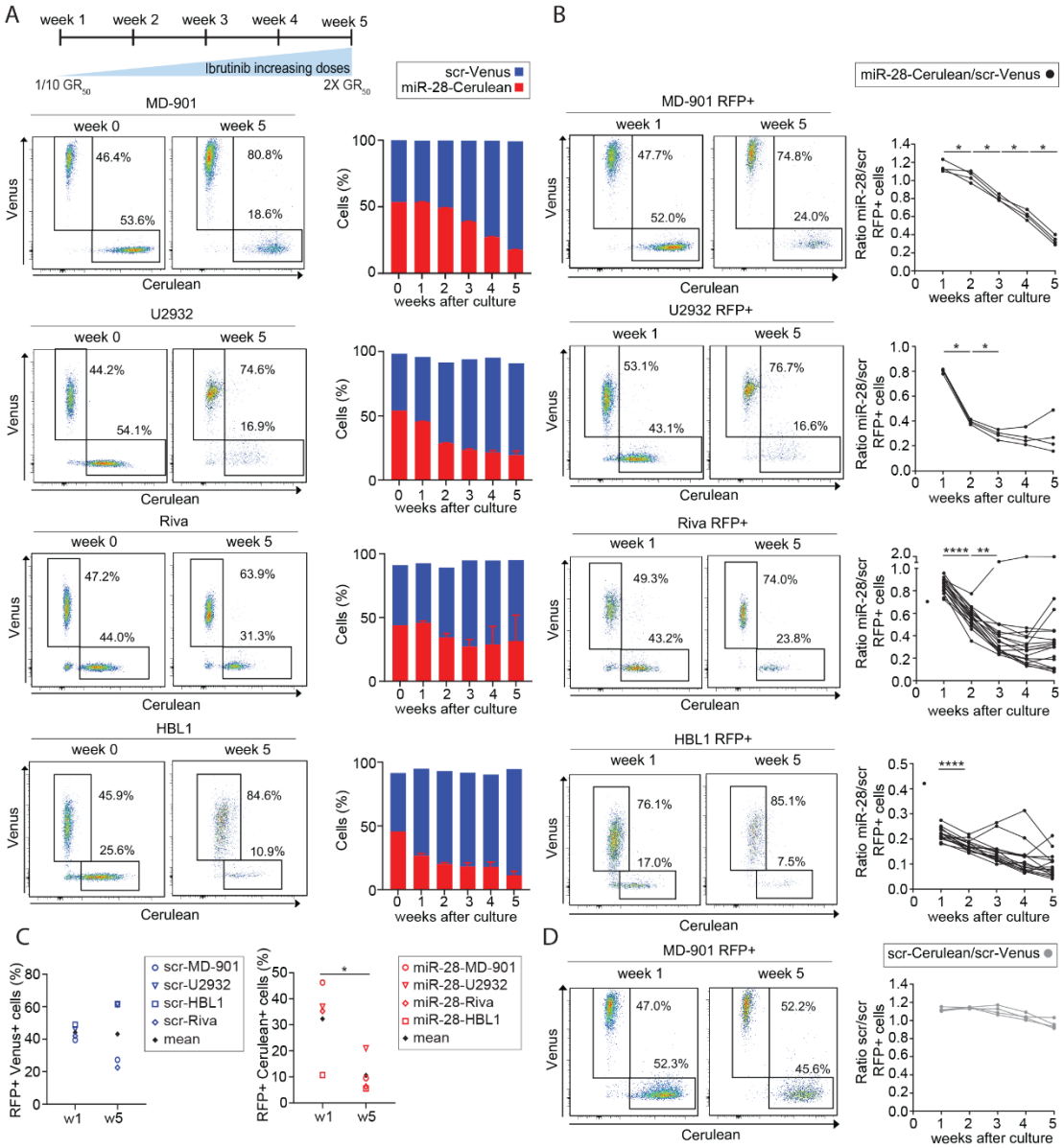

Figure 1. miR-28 limits the generation of ibrutinib resistance in polyclonal DLBCL cell competition assays.

Polyclonal ibrutinib-resistance competition assays were performed by mixing ABC-DLBCL cells transduced with doxycycline-inducible RFP expressing lentiviral vectors encoding either miR-28 or a scramble (scr) sequence and labeled with either Cerulean or Venus fluorescent proteins at a 1:1 ratio. Cultures were exposed to ibrutinib for five weeks, with the drug concentration increasing weekly to reach up to 2-fold above the ibrutinib GR_{50}. **(A–B)** Representative flow cytometry plots of scr-Venus/miR-28-Cerulean co-cultures and their evolution over five weeks in MD-901, U2932, Riva, and HBL1 cell lines. The bar chart (A) shows the progression of the total miR-28-Cerulean and scr-Venus populations over time. The graphs on the right (B) display the growth ratio of miR-28-Cerulean to scr-Venus within the RFP^+ population. **(C)** Percentage of RFP^+ cells in co-cultures with either scr-Venus (left) or miR-28-Cerulean (right) at weeks 1 and

5 of cell competition in the presence of ibrutinib, across four DLBCL cell lines. **(D)** Cell competition assay of scr-Venus/scr-Cerulean MD-901 cells cultured with increasing doses of ibrutinib for five weeks. Representative flow cytometry plots of the co-cultures (left) and percentage of MD-901 RFP^{+} populations over time (right). Statistical analysis: unpair *t*-test. **P*<0.05, ***P*<0.01, ****P*<0.0001.

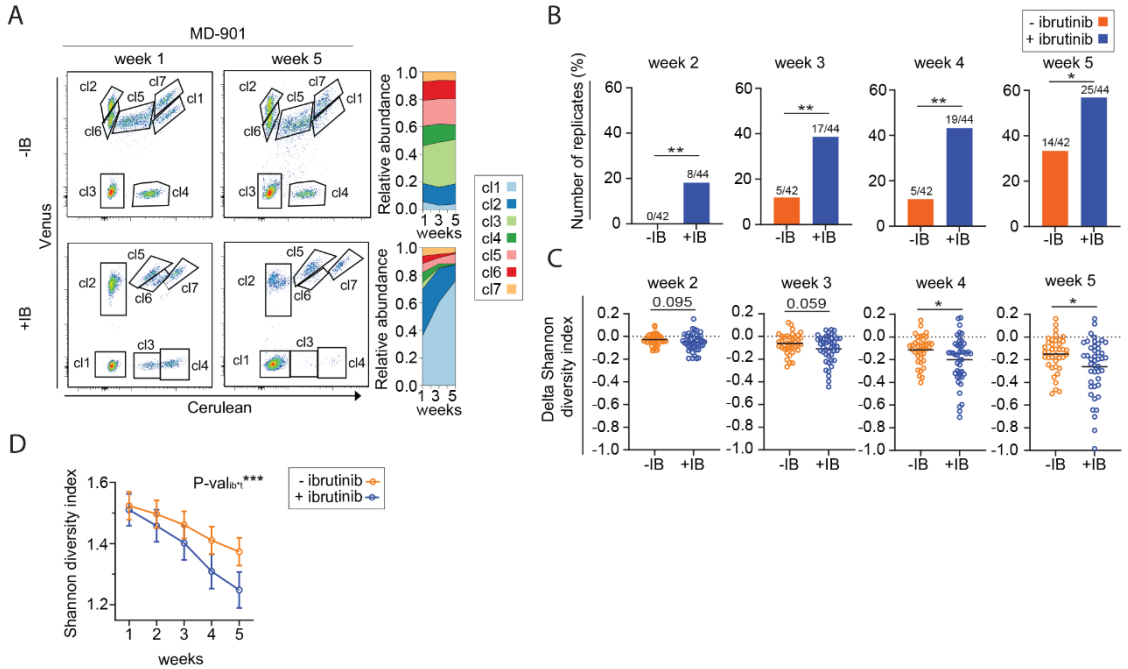

Figure 2. Flow cytometry-based clonal analysis reveals selection during acquisition of ibrutinib resistance in DLBCL.

Multicolor-labeled MD-901 ABC-DLBCL (MCL) cells, each carrying a random number of Venus- and/or Cerulean-encoding lentiviral constructs, were seeded into 96-well plates at an average density of 10 cells per well. Cells were then cultured for five weeks with ibrutinib, whose concentration increased weekly from 10-fold below to 2-fold above the GR_{50}, or left untreated (n = 45 wells/condition). **(A)** Representative wells showing clonal composition after one (left) or five (right) weeks under ibrutinib (+IB; well 1C) or control (-IB; well 11C) conditions, analyzed by flow cytometry. Clone proportions in these wells over time are shown in the Muller plot on the right. **(B)** Percentage of wells with changes in clone proportions compared to week one under +IB (blue) or -IB (orange) conditions. A significant change was defined as a >3-fold decrease at weeks 2–3, and >5-fold at weeks 4–5. **(C–D)** Clonal diversity measured by the Shannon index in wells treated with ibrutinib (blue) or left untreated (orange). Relative diversity per week, normalized to week 1 (C). Absolute Shannon diversity values over time (D). Error bars represent standard deviation (n = 45 wells/condition). Statistical analysis: Fisher's exact test (B), unpaired t-test (C), and two-way ANOVA (D). **P* < 0.05; ***P* < 0.01; ****P* < 0.001.

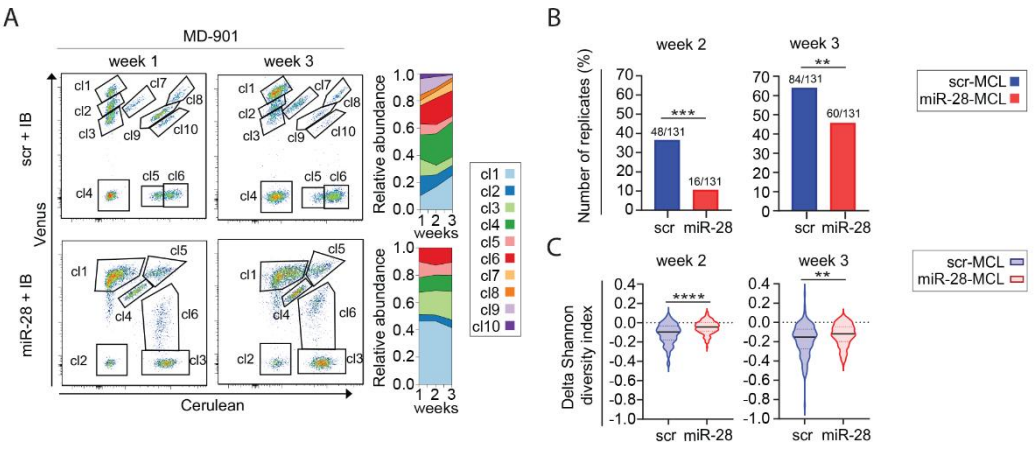

Figure 3. miR-28 inhibits clonal selection during acquisition of ibrutinib resistance in DLBCL cells.

Multicolor-labeled MD-901 ABC-DLBCL (MCL) cells transduced with doxycycline-inducible RFP-expressing lentiviral vectors encoding either miR-28 or a scramble control (scr) were seeded at an average density of 10 cells per well and exposed to gradually increasing concentrations of ibrutinib (IB) (n=45 wells/condition), as described in figure 2. **(A)** Representative wells showing clonal composition after one (left) or three (right) weeks in scramble (scr+IB; well 9A) or miR-28 (miR-28+IB; well 5D) cultures, analyzed by flow cytometry. Clone proportions over time in each well are shown in the Muller plots on the right. **(B)** Percentage of wells with significant changes in clone proportions compared to week 1 in scr (blue) or miR-28 (red) conditions. A significant change was defined as a >3-fold decrease. **(C)** Clonal diversity over time measured by the Shannon index, normalized to week 1, in scr (blue) and miR-28 (red) MCL wells. Statistical analysis: Fisher's exact test (B) and unpaired t-test (C). $^{**}P < 0.01$; $^{***}P < 0.001$; $^{****}P < 0.0001$.

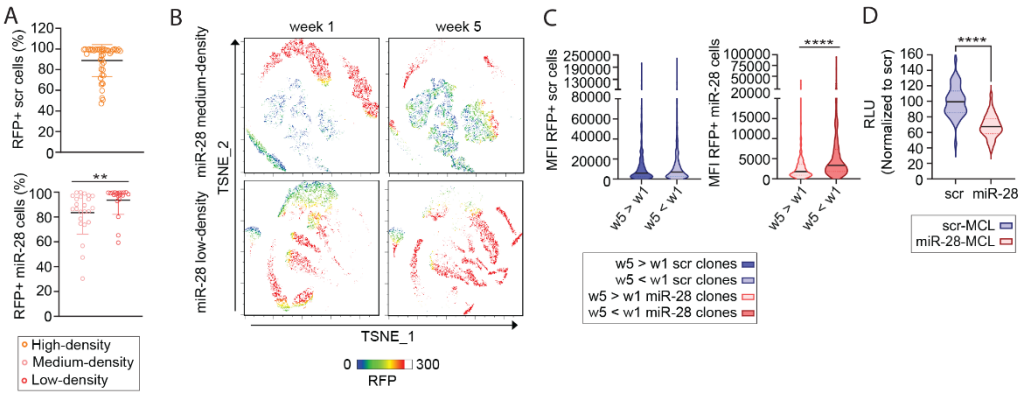

Figure 4. miR-28 interferes with the development of ibrutinib resistance in DLBCL cells.

Multicolor-labeled MD-901 ABC-DLBCL (MCL) cells transduced with doxycycline-inducible, RFP-expressing lentiviral vectors encoding either miR-28 or a scramble control (scr) were seeded at an average of 10 cells per well and exposed to increasing concentrations of ibrutinib (IB), reaching 2-fold above the GR_{50} after five weeks (n = 45 wells/condition and experiment). **(A)** Quantification of the percentage of RFP^+ cells in wells grouped by cellular density: high (orange), medium (pink), or low (red). **(B)** Representative examples of medium-density (well 5C) and low-density (well 5D) wells from the miR-28 group. FACS data from weeks 1 and 5 were concatenated and analyzed by t-SNE. Color gradient indicates RFP intensity. **(C)** Quantification of RFP mean fluorescence intensity (MFI) per clone, categorized by increased (w5 > w1) or decreased (w5 < w1) abundance at week 5 relative to week 1. Data pooled from three independent experiments. **(D)** Viable cell numbers in scr (left) and miR-28-expressing (right) wells at week 5, determined using CellTiter-Glo®. Luminescence was expressed as Relative Luminescence Units (RLU) and normalized to the mean of scr wells. Error bars represent standard deviation. Statistical analysis: unpaired t-test. $^{**}P < 0.01$ $^{****}P < 0.0001$.

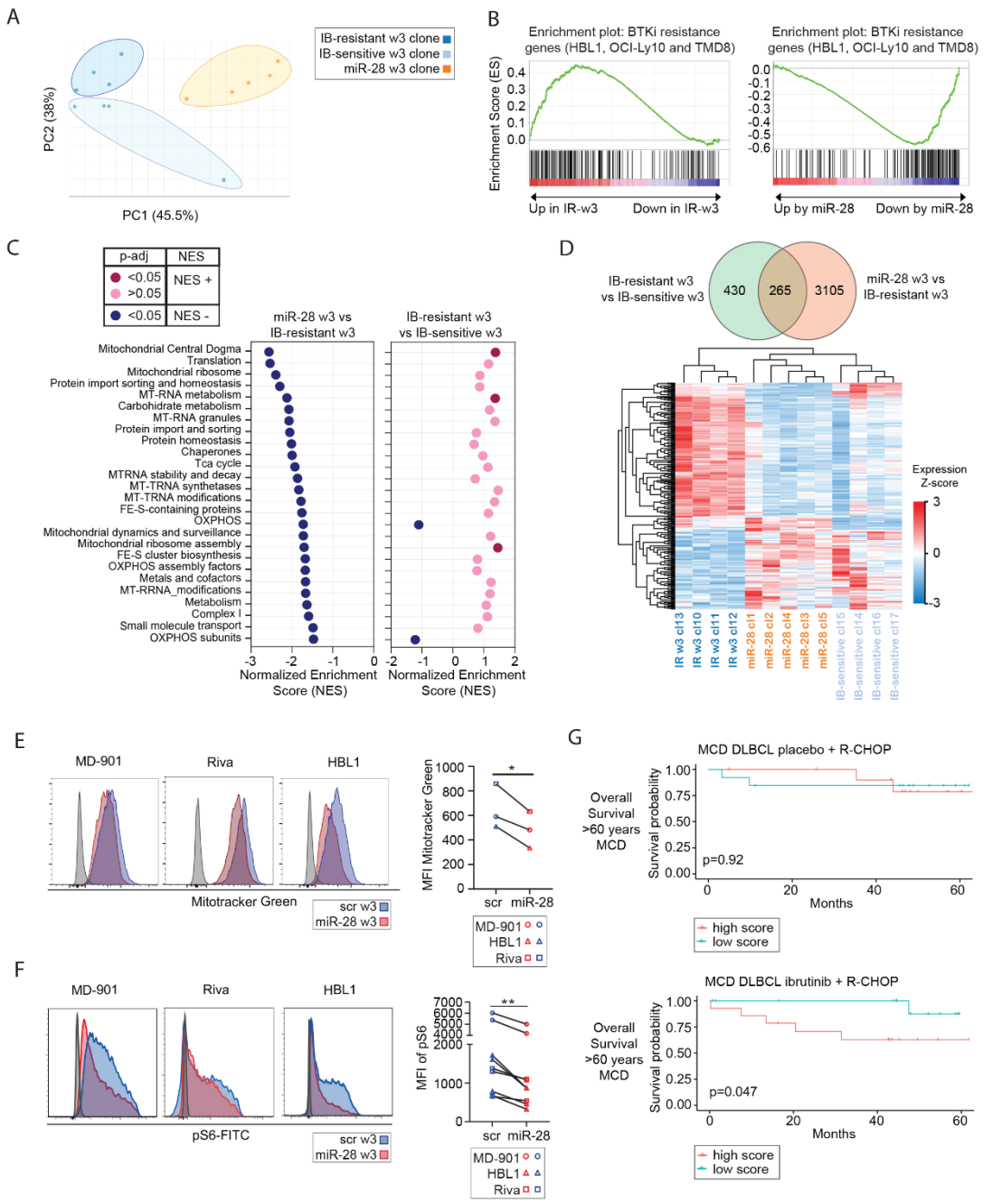

Figure 5. miR-28 suppresses pathways involved in ibrutinib resistance in ABC-DLBCL.

(A–D) Transcriptomic analysis of sorted multicolor-labeled MD-901 (MCL) clones after three weeks (w3) of culture with gradually increasing concentrations of ibrutinib (IB). MCL cells transduced with doxycycline-inducible, RFP-expressing lentiviral vectors encoding either miR-28 or a scramble control (scr) were seeded at an average density of 10 cells per well and exposed to IB, as described in Figure 2. **(A)** Principal component analysis of scr ibrutinib-resistant (IR) w3 clones (dark blue, n = 4), scr ibrutinib-sensitive w3 clones (light blue, n = 4), and miR-28–expressing (orange, n = 5) MCL clones. **(B)** Gene Set Enrichment Analysis (GSEA) of a BTK inhibitor resistance-essential gene set[21] in IR and miR-28 w3 MCL clones (FWER p = 0.003, FDR q = 0.003, NES = 1.42 in IR

w3 vs. ibrutinib-sensitive w3; FWER p = 0.000, FDR q = 0.000, NES = −2.21 in miR-28 w3 vs. IR w3). **(C)** GSEA of mitochondrial-related pathways (Mitocarta 3.0) in miR-28 and IR w3 MCL clones. Normalized enrichment scores (NES) and adjusted p-values (Benjamini–Hochberg correction) of altered pathways are shown in a scatter plot (blue dots, inhibited; pink dots, activated). **(D)** Heatmap showing hierarchical clustering based on Z-score expression values of the 265 genes involved in the acquisition of ibrutinib resistance and regulated by miR-28 in MD-901 clones. **(E–F)** Flow cytometry analysis of mitochondrial mass (E), assessed using MitoTracker Green staining, and S6 phosphorylation (F) in bulk miR-28- or scr-transduced MD-901, Riva, and HBL1 ABC-DLBCL cell lines after 3 weeks of culture in the presence of increasing doses of ibrutinib. Left: representative flow cytometry plots for each cell line (blue: scramble control; red: miR-28 overexpression; grey: unstained control). Right: Mean Fluorescence Intensity (MFI). Unpaired t-test; $*P < 0.05$; $P < 0.01$. **(G)** Kaplan–Meier analysis of overall survival in MCD DLBCL patients aged ≥60 (n = 54), stratified by a scored miR-28–IR gene signature in baseline biopsies from the PHOENIX trial[12], comparing patients treated with R-CHOP and R-CHOP plus ibrutinib: highest 50th percentile (up, red), and lowest 50th percentile (down, green). $*P < 0.05$ (Log-rank Mantel–Cox test).

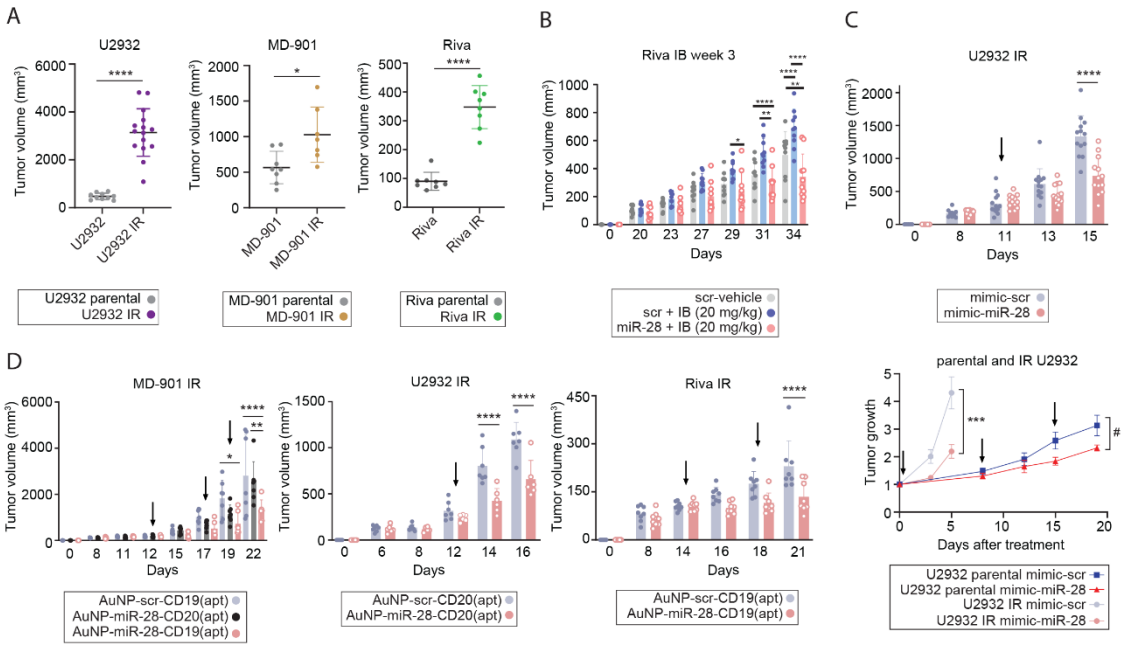

Figure 6. miR-28 suppresses the emergence and growth of ibrutinib-resistant DLBCL tumors in xenograft models.

(A) Tumor volume of parental and ibrutinib-resistant ABC-DLBCL cell lines: U2932 (16 days post-injection; parental: n = 10, IR: n = 15), MD-901 (17 days post-injection; parental: n = 8, IR: n = 7), and Riva (23 days post-injection; parental: n = 8, IR: n = 8) in xenograft models using NOD scid gamma (NSG) mice. Data represent mean tumor volume ± SD. **(B)** Tumor volumes of scramble (scr; control) and miR-28–expressing Riva cell xenografts in NSG mice treated or untreated with ibrutinib. scr and miR-28–transduced Riva cells were co-cultured *in vitro* for 3 weeks in the presence of doxycycline and increasing concentrations of ibrutinib. RFP^+ cells were sorted and injected subcutaneously into NSG mice, which received daily ibrutinib (20 mg/kg) or vehicle via oral gavage, and doxycycline in drinking water. Graph shows tumor volumes: scr tumors in vehicle-treated mice (gray dots, n = 10), scr tumors in ibrutinib-treated mice (blue dots, n = 10), and miR-28 tumors in ibrutinib-treated mice (pink dots, n = 10). Data represent mean ± SD. **(C)** Tumor volume of IR and parental U2932 xenografts in NSG mice treated intratumorally with miRNA mimics—miR-28 (light pink, n = 13) or scramble control (light blue, n = 13). Top graph: tumor volumes of U2932 IR xenografts. Data represent mean tumor volume ± SD. Bottom graph: tumor growth after treatment of U2932 IR tumors (miR-28: light pink, n = 13; scr: light blue, n = 13) and parental U2932 tumors (miR-28: red, n = 9; scr: dark blue, n = 10). Arrows indicate dosing schedules. Data represent mean ± SEM. **(D)** Tumor volumes of IR ABC-DLBCL xenografts treated intratumorally with CD19- or CD20-targeted gold nanoparticles (AuNPs): MD-901 IR (scr-CD19: n = 7; miR-28-CD20: n = 7; miR-28-CD19: n = 6), Riva (scr-CD19: n = 8; miR-28-CD19: n = 8), and U2932 (scr-CD20: n = 6; miR-28-CD20: n = 7). AuNP–miR-28 with cell line–specific aptamers (apt) (light pink), AuNP–miR-28 with non-specific apt (black), and AuNP–scramble with specific apt (light blue). Data represent mean ± SD. Arrows indicate dosing schedules. Statistical analysis: unpaired t-test (A); one-way

ANOVA (B, C top graph, D); two-way ANOVA (C bottom graph). # or *$P < 0.05$; **$P < 0.01$; ***$P < 0.001$; ****$P < 0.0001$.

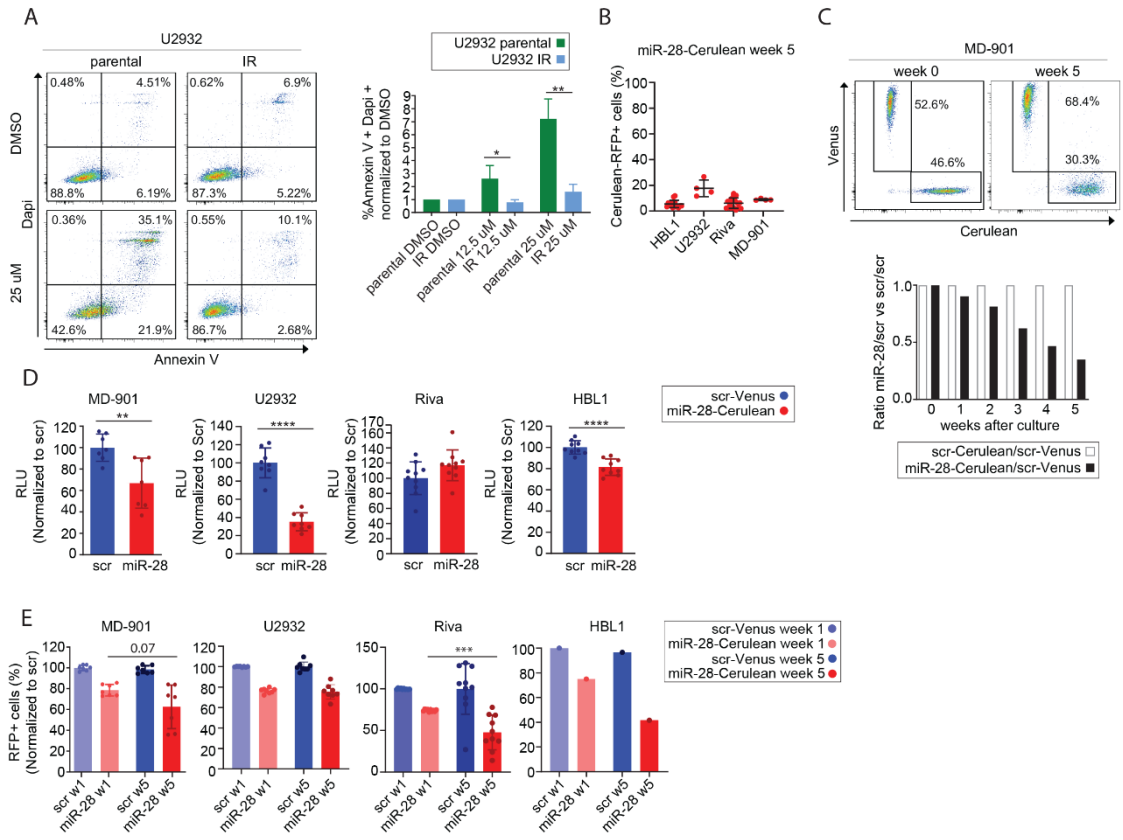

Figure S1. miR-28 suppresses ibrutinib resistance development in different ABC-DLBCL cell lines.

(A) Cell death analysis by flow cytometry in parental and IR U2932 ABC-DLBCL cells analyzed after three days of culture in the presence or absence of ibrutinib. Representative Annexin V and DAPI flow cytometry plots (left). Proportion of dead cells (Annexin V^+ $DAPI^+$) in parental (green) and IR (blue) U2932 cells (right). **(B-C)** Polyclonal ibrutinib-resistance competition assays were performed by mixing ABC-DLBCL cells transduced with doxycycline-inducible RFP-expressing lentiviral vectors encoding either miR-28 or a scramble (scr) sequence and labeled with either Cerulean or Venus fluorescent proteins at a 1:1 ratio. Cultures were exposed to ibrutinib for five weeks, with the drug concentration increasing weekly to reach up to 2-fold above the ibrutinib GR_{50}. (B) Quantification of miR-28-Cerulean RFP^+ cells exposed to ibrutinib for five weeks in polyclonal competition miR-28-Cerulean/scr-Venus assays of U2932 (n = 4), MD-901 (n = 4), Riva (n = 17) and HBL1 (n = 15) ABC-DLBCL cells. (C) Representative flow cytometry plots of scr-Venus/scr-Cerulean co-cultures and their evolution up to week 5 in MD-901 cells. Bottom graph represents the growth ratio of miR-28-Cerulean/scr-Venus co-cultures and their evolution up to week 5, normalized to the week 0 ratio and then to scr-Venus/scr-Cerulean cells in the MD-901 DLBCL cell line. **(D-E)** Analysis of

scr and miR-28 cultures grown for five weeks with increasing ibrutinib doses in four different ABC-DLBCL cell lines. (D) Viable cell number was determined at week 5 with CellTiter-Glo® reagent. (E) Graphs show the percentage of RFP$^+$ cells after one or five weeks in the presence of ibrutinib: week 1 scr-RFP$^+$ (light blue), week1 miR-28-RFP$^+$ (light red), week 5 scr-RFP$^+$ (dark blue) and week 5 miR-28-RFP$^+$ (dark red). Statistical analysis: t-test. *P<0.05, **P<0.01, *** P<0.001, ****P<0.0001. Error bars denote SD.

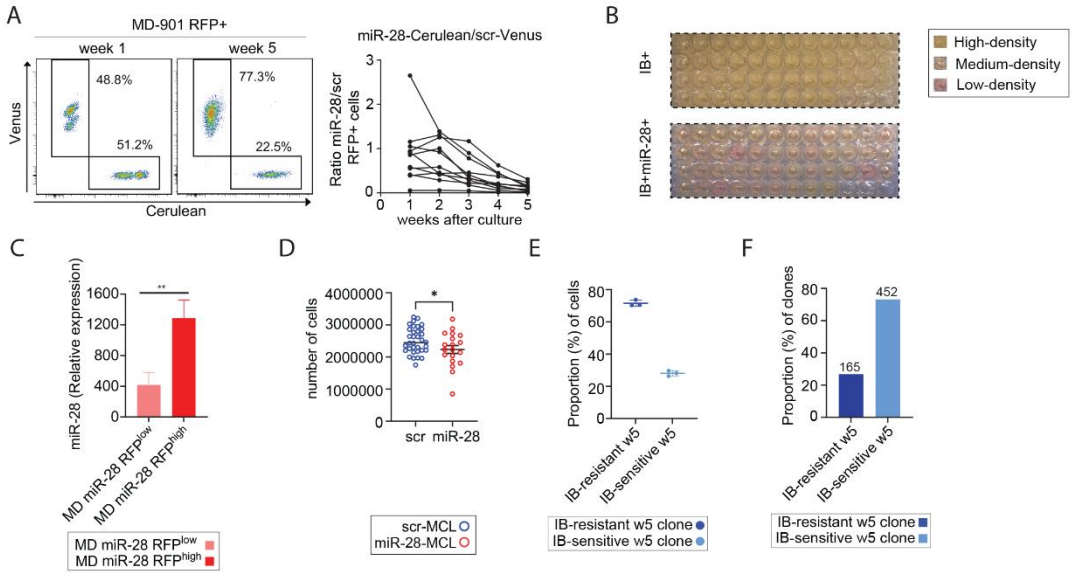

Figure S2. miR-28 impairs the development of ibrutinib resistance in ABC-DLBCL cells.

MD-901 ABC-DLBCL cells were transduced with doxycycline-inducible, RFP-expressing lentiviral vectors encoding either miR-28 or a scramble (scr) sequence, and labeled with Cerulean and/or Venus fluorescent proteins. Cells were seeded at an average density of 10 cells per well and exposed to increasing concentrations of ibrutinib (IB), reaching up to 2-fold the GR_{50} after five weeks. Clonal ibrutinib resistance competition assays are shown in (A), and multicolor-labeled MD-901 DLBCL (MCL) data are shown in (B, D-F). **(A)** Representative flow cytometry plots of RFP$^+$ cells in scr–Venus/miR-28–Cerulean co-cultures over five weeks. The bar chart displays the growth ratio of miR-28–Cerulean to scr–Venus within the RFP$^+$ population. **(B)** MCL wells after five weeks of ibrutinib exposure are classified as high-density, medium-density or low-density. Quantification is shown in Figure 4A. **(C)** Quantification of miR-28 expression in MD-901 ABC-DLBCL cells analyzed by qRT-PCR. RFP$^+$ cells from polyclonal miR-28-pTRIPZ MD-901 cultures were sorted according to their relative RFP expression levels after three days in the presence of doxycycline, and relative expression was normalized to the mean expression in scramble-pTRIPZ MD-901 cells. Error bars denote SD of 3 independent wells. **(D)** Number of viable cells in scr (left) and miR-28–expressing (right) wells with more than 80% RFP$^+$ cells after five weeks of culture, quantified using a

Countess 3 Automated Cell Counter. Error bars represent SEM. **(E-F)** Proportion of ibrutinib-resistant (defined as week 5 > week 1) and ibrutinib-sensitive (defined as week 5 < week 1) cells (E) or clones (F) in MCL wells after five weeks of culture, compared to week 1 (n = 3 experiments; 45 wells per experiment). Error bars represent SD. Statistical analysis: unpaired t-test. *$P < 0.05$.

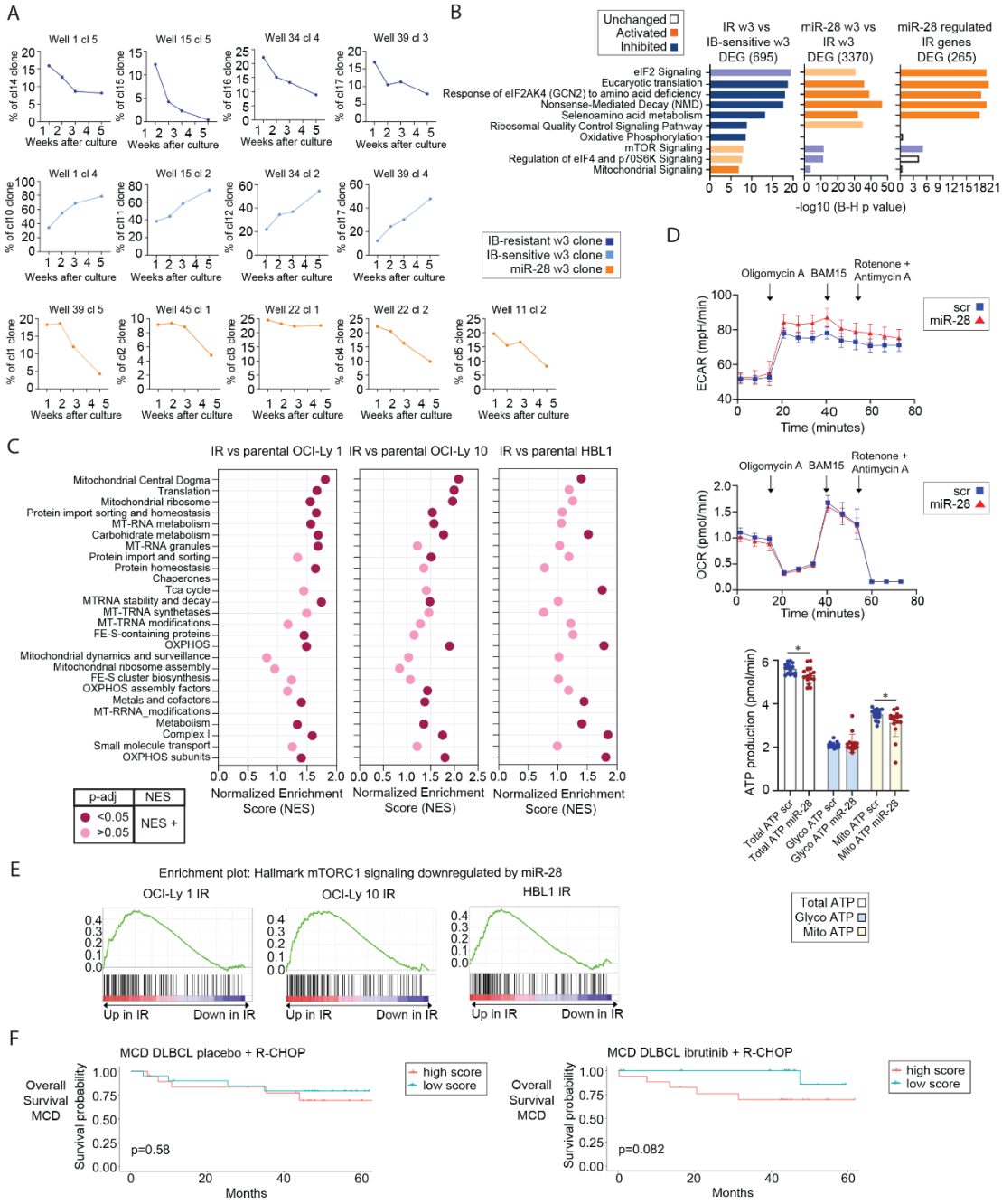

Figure S3. miR-28 regulates metabolic programs associated with ibrutinib resistance.

(A–C) Transcriptomic analysis of sorted multicolor-labeled MD-901 (MCL) clones after three weeks (w3) of culture with gradually increasing concentrations of ibrutinib (IB). MCL cells transduced with doxycycline-inducible, RFP-expressing lentiviral vectors encoding either miR-28 or a scramble (scr) control were seeded at an average density of 10 cells per well and exposed to ibrutinib, as described in Figure 2. **(A)** Graphs show the proportion of scr ibrutinib-sensitive clones, scr ibrutinib-resistant clones, and miR-28–expressing MCL clones used for RNA-seq after five weeks of ibrutinib exposure. **(B)** Graphs display the top 10 significantly altered pathways identified by Ingenuity Pathway Analysis (IPA) in the comparison between ibrutinib-resistant and ibrutinib-sensitive w3 clones (left). Pathway activity is also shown for the comparisons of miR-28 vs. ibrutinib-resistant w3 clones (middle) and the miR-28–regulated IR gene signature (right). Predicted pathway activity is indicated by color (blue: inhibited; orange: activated; white: non-predicted). P-values were adjusted for multiple testing using the Benjamini–Hochberg false discovery rate (FDR) method. **(C)** GSEA of mitochondrial-related pathways (Mitocarta 3.0) in ibrutinib-resistant (IR) versus parental OCI-Ly1, OCI-Ly10, and HBL1 cells[33]. Normalized enrichment scores (NES) and adjusted p-values (Benjamini–Hochberg correction) for significantly altered pathways are displayed in a scatter plot. Activated pathways are highlighted in pink. **(D)**. Oxygen consumption rate (OCR) and extracellular acidification rate (ECAR) measurements in miR-28– and scr-expressing MD-901 cells after three weeks of culture in the presence of gradually increasing concentrations of ibrutinib (miR-28: red; scr: blue). OCR and ECAR were measured before and after sequential injections of oligomycin A, BAM15, and rotenone plus antimycin A. Arrows indicate the timing of each injection. The chart shows ATP production rates: total (white), glycolytic (blue), and mitochondrial (yellow). Statistical analysis: unpaired t-test. $*P < 0.05$. **(E)** Gene Set Enrichment Analysis (GSEA) of the "Hallmark mTORC1 signaling" pathway (as defined by GSEA), showing downregulation by miR-28 in MCL MD-901 clones. Comparisons were made between IR and parental OCI-Ly1, OCI-Ly10, and HBL1 cells[33]. Significant enrichment was observed in IR cells **(F)** Kaplan–Meier analysis of overall survival in MCD DLBCL patients (n = 73), stratified by miR-28–IR gene signature score in baseline biopsies from the PHOENIX trial[12]. Patients were treated with R-CHOP or R-CHOP plus ibrutinib. Groups correspond to the highest 50th percentile (up, red) and lowest 50th percentile (down, green). Statistical test: Log-rank (Mantel–Cox).

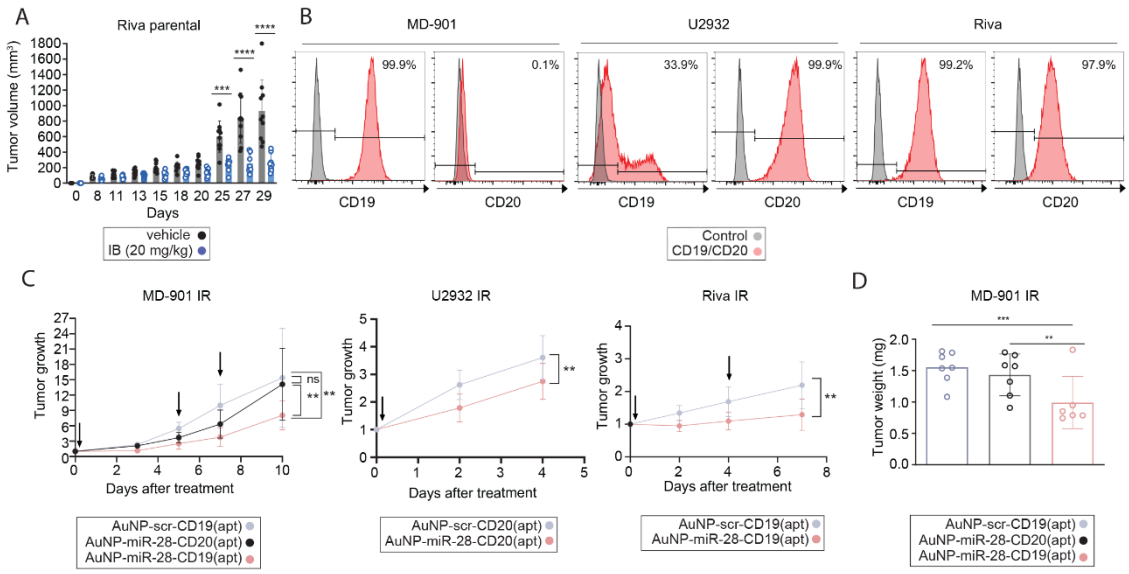

Figure S4. Aptamer-targeted delivery of miR-28 suppresses the growth of ibrutinib-resistant DLBCL tumors in xenograft models.

(A) Tumor volume of parental Riva DLBCL cells in xenograft models in NSG mice treated daily with ibrutinib (20 mg/kg, n = 8) or vehicle (n = 10) via oral gavage. **(B)** CD19 and CD20 expression in MD-901, U2932, and Riva cell lines analyzed by flow cytometry. **(C–D)** Ibrutinib-resistant DLBCL cells were generated following the protocol described in Figure 1. (C) Tumor growth of ibrutinib-resistant (IR) ABC-DLBCL xenografts treated intratumorally with CD19- or CD20-targeted gold nanoparticles (AuNPs): AuNP–miR-28 with specific aptamers (light pink), AuNP–miR-28 with nonspecific aptamers (black), and AuNP–scr with specific aptamers (light blue). Arrows indicate dosing schedules. (D) Tumor weight measured at endpoint in IR MD-901 xenografts treated with: AuNP–scr–CD19 (light blue), AuNP–miR-28–CD20 (black), and AuNP–miR-28–CD19 (light pink). Statistical analysis: one-way ANOVA (A); two-way ANOVA (C); unpaired t-test (D). $^{**}P < 0.01$; $^{***}P < 0.001$; $^{****}P < 0.0001$. Data represent mean ± SD.
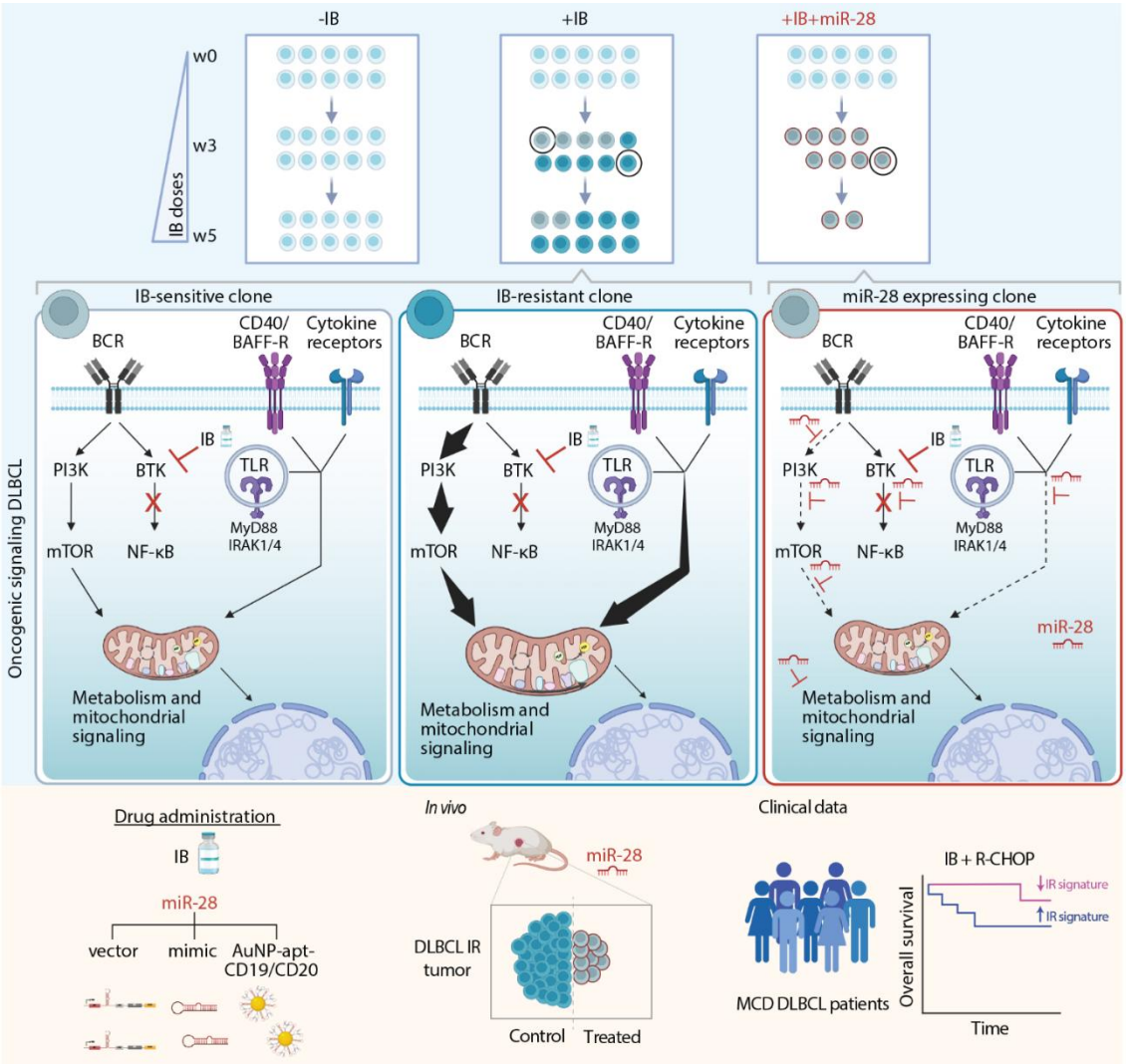
Graphical abstract